Nature Communications

https://doi.org/10.1038/s41467-026-75102-9

Article in Press

Glutamatergic signaling underlies brain structural organization for mathematical and reading abilities in children

Received: 20 October 2025

Accepted: 18 June 2026

Published online: 04 July 2026

Cite this article as: Zhang, Y., Chang, H., El-Said, D. *et al.* Glutamatergic signaling underlies brain structural organization for mathematical and reading abilities in children. *Nat Commun* (2026). https://doi.org/10.1038/s41467-026-75102-9

Yuan Zhang, Hyesang Chang, Dawlat El-Said & Vinod Menon

Glutamatergic signaling underlies brain structural organization for mathematical and reading abilities in children

Yuan Zhang[1], Hyesang Chang[1], Dawlat El-Said[1], Vinod Menon[1,2,3,4]**

[1]Department of Psychiatry & Behavioral Sciences, Stanford University, Stanford, CA 94305, USA.
[2]Department of Neurology & Neurological Sciences, Stanford University, Stanford, CA 94305, USA.
[3]Stanford Wu Tsai Neurosciences Institute, Stanford University, Stanford, CA 94305, USA.
[4]Graduate School of Education, Stanford University, Stanford, CA 94305, USA.

*Corresponding authors: Yuan Zhang; Vinod Menon. Email: yuanzh@stanford.edu; menon@stanford.edu

Abstract

The neurochemical mechanisms underlying individual differences in children's mathematical and reading abilities remain largely unknown. Here we investigate how neurotransmitter systems relate to brain structural organization supporting these abilities in two independent cohorts of children (*N*=991). We mapped brain-wide structural phenotypes associated with academic performance onto a comprehensive PET atlas of 19 neurotransmitter receptors and transporters. Across both domains and cohorts, NMDA glutamatergic receptor distribution showed the most consistent associations with brain structural organization supporting academic abilities (replication Bayes factors >9e4 for mathematics; >4 for reading). NMDA receptor density corresponded with multiple functional networks for mathematical abilities but showed more spatially focused associations within visual networks for reading, suggesting both shared and domain-specific neurochemical mechanisms. Dopaminergic, cholinergic, serotonergic, and GABAergic systems showed weaker, non-replicable associations. These findings bridge molecular neurochemistry and macro-scale brain architecture supporting academic skills, identifying glutamatergic signaling as a candidate target for interventions addressing learning disabilities.

Introduction

Mathematics and reading are fundamental pillars of children's cognitive development, serving as essential skills for everyday functioning and academic achievement [1]. Proficiency in these domains is acquired over extended educational experience and strongly predicts professional success and economic growth [2,3]. However, substantial variability exists in the development of these skills, with learning disabilities affecting approximately 20% of school-aged children globally [4]. This prevalence underscores a critical question in developmental cognitive neuroscience: what molecular substrates contribute to individual differences in mathematical and reading abilities?

While decades of neuroimaging research have identified brain regions and networks supporting mathematical [5-11] and reading [12] abilities, a fundamental gap exists in our understanding of the molecular substrates that support these neural systems. This gap represents a major barrier to advancing both our theoretical understanding of cognitive development and our ability to develop effective interventions for learning difficulties. The molecular level is particularly important because neurotransmitter systems – the brain's primary signaling mechanisms – not only mediate neural communication but also shape brain development and plasticity, making them potential targets for intervention [13,14].

Neurotransmitters are key signaling molecules that shape both neural architecture and cognitive function through multiple mechanisms [15-17]. Beyond their classical role in synaptic transmission, neurotransmitters guide neural development by influencing cell differentiation, neuronal

migration, and synaptic formation [18]. As the brain matures, these molecular systems continue to influence neural plasticity, learning, and memory formation, all processes critical for developing complex cognitive skills like mathematics and reading. Understanding how different neurotransmitter systems relate to brain organization supporting these cognitive abilities could fundamentally transform our approach to learning and its difficulties.

The two primary neurotransmitter systems in the brain – glutamate and GABA (γ-aminobutyric acid) – are particularly relevant for learning and cognitive development [19-27]. N-methyl-D-aspartate (NMDA) receptors, a key type of glutamate receptor, are crucial for synaptic plasticity and learning through their role in strengthening connections between neurons [28]. In parallel, GABA maintains optimal neural function by preventing excessive excitation and helping orchestrate the precise timing of neural activity [29]. The balance between these excitatory and inhibitory systems is critical for learning, with disruptions linked to various cognitive difficulties [30-38]. Other key modulatory systems include dopamine, which shapes reward-based learning, motivation, and cognitive flexibility [39-42], and serotonin, which influences mood and cognitive flexibility [43]. However, we lack understanding of how these various neurotransmitter systems work across the whole brain to support complex cognitive abilities like mathematics and reading.

Previous investigations of neurotransmitters in mathematical and reading abilities have primarily relied on magnetic resonance spectroscopy (MRS) [44,45] (see Supplementary Table 1 for a summary), a non-invasive method that provides in vivo, individual-specific measures of metabolite concentrations within targeted regions. This makes MRS particularly valuable for characterizing individual differences in neurochemical levels within a study sample. Using this

approach, prior studies have yielded important insights: glutamate and GABA levels in the intraparietal sulcus and middle frontal gyrus predict mathematical performance [37,46,47], with developmental changes in these relationships suggesting age-specific effects. In reading research, glutamate levels in the occipital cortex and anterior cingulate and GABA concentration in the inferior frontal gyrus were associated with reading performance in children [48-50].

However, several important methodological limitations constrain the field. Traditional MRS studies are typically restricted to one or a small number of pre-selected brain regions per acquisition, and while recent advances now enable broader spatial coverage [51], these approaches remain limited in their ability to simultaneously characterize the full diversity of neurotransmitter receptor subtypes across the whole brain. A further important constraint is that MRS measures the total metabolite pool within a voxel, reflecting contributions from synaptic, extrasynaptic, and metabolic compartments, and tightly coupled to the neuron–astrocyte glutamate–glutamine cycle, making it difficult to draw specific conclusions about receptor-mediated signaling from MRS data alone [52]. Beyond these technical constraints, other neurotransmitter systems crucial for learning and motivation, including dopamine, serotonin, and acetylcholine, remain largely unexplored in the context of mathematical and reading abilities. No studies have concurrently investigated neurotransmitter contributions to both mathematical and reading abilities, and replication efforts have been minimal, raising questions about the reliability of existing findings.

Recent advances in positron emission tomography (PET) imaging now provide a complementary opportunity to characterize multiple neurotransmitter systems at the whole-brain level by measuring receptor densities and their spatial distributions across the entire brain [16,53-58]. While

MRS is well suited for identifying regionally localized, individual-level variation in neurochemical concentrations, PET offers a system-level framework for understanding the molecular architecture of the distributed brain networks that support mathematical and reading abilities. Specifically, PET can quantify the spatial distribution of specific neurotransmitter receptors and transporters throughout the brain [59], enabling tests of whether large-scale brain-behavior associations are spatially aligned with particular neurotransmitter systems. Using radioligands that selectively bind to different receptor types, PET has enabled measurement of multiple neurotransmitter systems, including glutamate [19-25,60], GABA [26,27,55,60], acetylcholine [16,54,61], dopamine [16,54,56], and serotonin [54-56]. However, because PET requires radiotracer administration and involves ionizing radiation, it is not well suited for direct acquisition in healthy pediatric samples.

In this context, the recent development of a comprehensive human brain atlas of multiple neurotransmitter systems [59] provides an unprecedented opportunity to examine how multiple molecular systems relate to individual differences in cognitive abilities. Constructed from PET imaging data from over 1,200 healthy individuals (mean ages 19.9-68.3 years), this atlas maps the distribution of 19 different neurotransmitter receptors and transporters across the whole brain at high spatial resolution [13,62]. By leveraging this atlas as a normative spatial reference, we can characterize how receptor distribution patterns correspond to the brain structural organization supporting academic abilities. This atlas-based approach complements and extends what is possible with MRS alone by providing a whole-brain, system-level view of neurotransmitter architecture, while avoiding direct radiotracer administration in children.

In the present study, we address the critical gap between molecular substrates and cognitive abilities by examining how multiple neurotransmitter systems relate to brain structural organization supporting mathematical and reading abilities in children. Our analytical approach has two key components (Fig. 1). First, using structural MRI and Brainnetome atlas-based canonical correlation analysis (CCA), we identified whole-brain structural phenotypes associated with mathematical and reading abilities. These phenotypes are defined as multivariate patterns of associations between regional grey matter volume across the whole brain and mathematical or reading ability across participants, and their spatial expression is referred to here as brain structural organization. Second, we examined how these structural phenotypes map onto the spatial distribution of 19 neurotransmitter receptors and transporters, allowing us to identify which molecular systems most strongly correspond to brain structural organization supporting these cognitive abilities. To ensure robust and replicable findings, we employed a discovery-validation approach using two independent cohorts of children aged 7-14 years. The Child Mind Institute–Healthy Brain Network (CMI-HBN) discovery cohort (*N*=760) represents one of the largest neuroimaging studies of mathematical and reading abilities to date [63] for identifying reliable brain-behavior relationships in the developing brain. We then tested whether these relationships replicated in an independent Stanford validation cohort (*N*=231). By examining both mathematical and reading abilities within same participants using identical methods, we can directly compare how different neurotransmitter systems relate to brain structural organization supporting these distinct but related cognitive domains.

Grounded in the well-established excitatory-inhibitory (E/I) balance framework, which posits that optimal learning requires precise coordination between glutamate-mediated excitation and

GABA-mediated inhibition [31,38,64], we hypothesized that glutamate and GABA systems would show significant spatial correspondence with brain structural organization supporting both mathematical and reading abilities. This hypothesis was motivated by the established role of glutamatergic and GABAergic systems in neural plasticity and circuit refinement during childhood [30-38]. At the same time, while mathematical and reading abilities share substantial cognitive, genetic, and environmental architecture, including overlapping genetic risk factors, and co-occurring learning difficulties [65,66], the neural systems supporting these domains are not identical. We therefore further hypothesized that neurotransmitter systems would exhibit both convergent (domain-general) and partially dissociable (domain-specific) spatial associations with brain structural organization for mathematical versus reading abilities. Additionally, neurotransmitter systems including dopamine, serotonin, and acetylcholine, implicated in motivation, cognitive flexibility, learning, and attention, were predicted to show associations with brain structural organization across both domains. Finally, we predicted that neurotransmitter-brain structure associations would replicate consistently across both independent cohorts, providing evidence for robust and generalizable molecular signatures of cognitive abilities.

Our study provides a comprehensive characterization of the correspondence between neurotransmitter receptor distributions and brain structural organization supporting mathematical and reading abilities, bridging molecular and systems-level neuroscience. This bridge is crucial because it helps explain how the molecular basis of learning and plasticity relates to the development of large-scale brain networks supporting complex cognitive skills. More broadly, our findings contribute to a multi-level model of cognitive development that connects molecular

foundations to brain structure to behavior, providing a framework for understanding both typical development and learning difficulties.

Results

Behavioral characteristics and correlations

Given the known overlap between mathematical and reading abilities, we first examined their behavioral relationships using two-sided Pearson correlations in the CMI-HBN discovery cohort (N = 760) and then in the Stanford validation cohort (N = 231).

In the CMI-HBN discovery cohort, we examined the relationship between mathematical and reading abilities using standardized grade-normed scores from the WIAT-III (Table 1). Mathematical abilities were assessed using numerical operations and math problem-solving scores, and reading abilities were assessed using word reading and reading comprehension scores. Mathematical and reading abilities were highly correlated: numerical operations correlated with word reading (t(758) = 14.42, r = 0.46, 95% CI [0.41, 0.52], p = 7.7e-42) and reading comprehension (t(758) = 11.74, r = 0.39, 95% CI [0.33, 0.45], p = 2.4e-29); math problem solving showed even stronger correlations with word reading (t(758) = 17.48, r = 0.54, 95% CI [0.48, 0.58], p = 9.1e-58) and reading comprehension (t(758) = 16.98, r = 0.52, 95% CI [0.47, 0.57], p = 5.0e-55).

In the Stanford validation cohort, we examined whether these behavioral relationships were replicated. Using WIAT-II scores (Table 1), we again observed strong correlations between mathematical and reading abilities: numerical operations correlated with word reading ($t(229) = 8.04$, $r = 0.47$, 95% CI [0.36, 0.56], $p = 4.8e\text{-}14$) and reading comprehension ($t(229) = 7.72$, $r = 0.45$, 95% CI [0.35, 0.55], $p = 3.6e\text{-}13$); math reasoning showed stronger correlations with word reading ($t(229) = 10.37$, $r = 0.57$, 95% CI [0.47, 0.65], $p = 6.6e\text{-}21$) and reading comprehension ($t(229) = 9.76$, $r = 0.54$, 95% CI [0.44, 0.63], $p = 4.8e\text{-}19$).

The robust correlations between mathematical and reading abilities across both cohorts indicate substantial behavioral overlap between these domains, suggesting that subsequent brain-behavior analyses may capture both shared and partially dissociable components.

Brain structural organization associated with mathematical ability

To identify brain structural features associated with mathematical ability, we first characterized the multivariate relationships between brain structure and mathematical skills. We employed canonical correlation analysis (CCA) to examine relationships between grey matter volume across 218 brain regions and two measures of mathematical ability (numerical operations and math problem-solving/reasoning), while controlling for age.

In the CMI-HBN discovery cohort ($N = 760$), CCA revealed a significant relationship between brain structure and mathematical abilities (Pillai's trace = 0.34, permutation $p = 0.0002$), accounting for 31.5% of the shared variance between brain structure and mathematical performance. A robust canonical correlation ($r = 0.26$, bootstrap 95% CI [0.24, 0.36], FDR-

corrected permutation p = 3.0e-4) emerged between brain structure and mathematical ability. Both numerical operations and math problem-solving subtests contributed positively to this relationship (Fig. 2a). The brain-behavior associations were distributed across multiple regions, with the strongest positive associations observed in the insula, anterior cingulate cortex, prefrontal cortex, and posterior cingulate cortex (Supplementary Fig. 1a; Supplementary Table 2). Additional analyses confirmed that the brain-behavior relationships were stable across age groups and sexes, and remained robust after controlling for IQ, SES, site, and total brain volume (see Supplementary Notes).

In the Stanford validation cohort (N = 231), we successfully replicated the key findings from our discovery cohort. The CCA model again demonstrated a significant relationship between brain structure and mathematical abilities (Pillai's trace = 0.56, permutation p = 0.0002), accounting for 49.8% of the shared variance in the brain-behavior relationship. The brain-behavior mode showed a robust canonical correlation (r = 0.35, bootstrap 95% CI [0.31, 0.51], FDR-corrected permutation p = 3.0e-4) between brain structure and mathematical ability. Critically, the spatial pattern of brain-behavior relationships displayed remarkable consistency with that of the discovery cohort (Fig. 2b), involving similar brain regions and networks (Supplementary Fig. 1a; Supplementary Table 2). Again, the identified brain-behavior relationships were stable across age groups and sexes, and remained robust after controlling for IQ, SES, site, and total brain volume (see Supplementary Notes).

To directly test generalizability, we applied the CCA model derived from the discovery cohort to the validation cohort (see Methods), finding significant prediction of brain-behavior relationships (r = 0.19, bootstrap 95% CI [0.07, 0.30], permutation p = 0.002; Fig. 3a).

The replication of these brain-behavior relationships across two independent cohorts provides strong evidence for reliable associations between brain structure and mathematical ability. The distributed pattern of involved brain regions, particularly in prefrontal and cingulate areas, suggests that mathematical ability relates to structural variation across multiple functional networks rather than in isolated regions.

Neurotransmitter mapping for mathematical ability

Having established reliable brain structural phenotypes associated with mathematical ability, we next investigated which neurotransmitter systems might relate to its spatial expression. Specifically, we examined how the spatial distribution of 19 different neurotransmitter receptors and transporters mapped onto the CCA-derived brain structural organization, using linear regression with spatial autocorrelation-preserving permutation tests and Bayesian analyses to assess significance.

In the CMI-HBN discovery cohort, NMDA receptor distribution significantly mapped onto brain structural organization associated with mathematical ability (adjusted $R^2 = 0.15$, FDR-corrected spin-test $p = 0.013$, $BF_{10} = 4.0e6$). Two other neurotransmitter systems also showed significant associations: acetylcholine (VAChT: adjusted $R^2 = 0.34$, FDR-corrected spin-test $p = 0.002$, $BF_{10} = 2.0e18$) and histamine (H3: adjusted $R^2 = 0.24$, FDR-corrected spin-test $p = 0.002$, $BF_{10} = 6.0e11$). The spatial distribution of these receptors showed positive correlations with brain

regions where greater grey matter volume was associated with better mathematical ability (Fig. 4a).

In the Stanford validation cohort, NMDA receptor distribution again significantly mapped onto math-related brain structural organization (adjusted $R^2 = 0.20$, FDR-corrected spin-test $p = 0.001$, $BFr_{10} = 9.0e4$), along with several other neurotransmitter systems including $mGluR_5$, $GABA_{A/BZ}$, and dopamine receptors (Fig. 4b).

Notably, NMDA was the only neurotransmitter system that showed consistent relationships across both cohorts (Fig. 5a), as indicated by significant effects in both the discovery and validation samples. This cross-cohort consistency substantiates the role of glutamatergic signaling, particularly through NMDA receptors, in its association with brain structural organization supporting mathematical ability.

Network-level NMDA mapping for mathematical ability

Given NMDA's consistent relationship with mathematical ability across cohorts, we examined how these relationships manifested across different functional brain networks. This network-level analysis aimed to understand whether NMDA's influence showed network specificity.

In the CMI-HBN discovery cohort, NMDA receptor distribution showed significant positive correlations with math-related brain structural organization in four networks: dorsal default mode ($t(21) = 5.18$, $r = 0.75$, 95% CI [0.49, 0.89], FDR-corrected $p = 5.0e-4$), anterior ($t(22) = 3.96$, r

= 0.65, 95% CI [0.33, 0.83], FDR-corrected p = 0.004) and posterior salience (t(8) = 3.65, r = 0.79, 95% CI [0.32, 0.95], FDR-corrected p = 0.023), and higher-order visual networks (t(12) = 3.24, r = 0.68, 95% CI [0.24, 0.89], FDR-corrected p = 0.023) (Fig. 6a-d; Supplementary Table 3).

In the Stanford validation cohort, the network-level relationships observed in the discovery cohort were replicated in dorsal default mode (t(21) = 3.56, r = 0.61, 95% CI [0.27, 0.82], FDR-corrected p = 0.004), anterior (t(22) = 2.63, r = 0.49, 95% CI [0.11, 0.75], FDR-corrected p = 0.015) and posterior salience (t(8) = 3.16, r = 0.75, 95% CI [0.22, 0.94], FDR-corrected p = 0.015), and higher-order visual (t(12) = 3.88, r = 0.75, 95% CI [0.36, 0.91], FDR-corrected p = 0.004) networks (Fig. 6a-d; Supplementary Table 3).

The consistency of these network-level patterns across cohorts suggests a robust association between NMDA receptor distribution and mathematical ability across multiple functional networks.

Brain structural organization associated with reading ability

We next examined how brain structure relates to reading ability, allowing us to later compare molecular substrates across these cognitive domains. Using the same CCA approach, we examined relationships between grey matter volume and two measures of reading ability (word reading and reading comprehension), while controlling for age.

In the CMI-HBN discovery cohort, CCA revealed a significant relationship between brain structure and reading abilities (Pillai's trace = 0.31, permutation p = 0.0002), accounting for 29.5% of the shared variance between brain structure and reading. A robust canonical correlation (r = 0.22, bootstrap 95% CI [0.21, 0.33], FDR-corrected permutation p = 3.0e-4) emerged between brain structure and reading ability. Both word reading and reading comprehension subtests contributed positively to this relationship (Fig. 7a). Brain regions showing the strongest positive associations included prefrontal, ventral temporal-occipital, and posterior cingulate cortices, suggesting involvement of both reading-specific and domain-general networks (Supplementary Fig. 1b; Supplementary Table 4). Additional analyses confirmed that the brain-behavior relationships were stable across age groups and sexes, and remained robust after controlling for IQ, SES, site, and total brain volume (see Supplementary Notes).

In the Stanford validation cohort, we successfully replicated the key findings from our discovery cohort. The CCA model again demonstrated a significant relationship between brain structure and reading abilities (Pillai's trace = 0.57, permutation p = 0.0002), accounting for 50.1% of the shared variance in the brain-behavior relationship. The brain-behavior mode showed a robust canonical correlation (r = 0.34, bootstrap 95% CI [0.32, 0.51], FDR-corrected permutation p = 0.001) between brain structure and reading ability. Critically, the spatial pattern of brain-behavior relationships displayed remarkable consistency with that of the discovery cohort (Fig. 7b), involving similar brain regions and networks (Supplementary Fig. 1b; Supplementary Table 4). Again, the identified brain-behavior relationships were stable across age groups and sexes, and remained robust after controlling for IQ, SES, site, and total brain volume (see Supplementary Notes).

To formally test generalizability, we applied the CCA model derived from the discovery cohort to the validation cohort (see Methods), finding significant prediction of brain-behavior relationships (r = 0.16, bootstrap 95% CI [0.04, 0.28], permutation p = 0.007; Fig. 3b).

The replication of these brain-behavior relationships across two independent cohorts establishes reliable associations between brain structure and reading ability. While some involved regions overlap with those identified for mathematical ability, including prefrontal and posterior cingulate cortices, others appear more specific to reading (e.g., ventral temporal-occipital cortex). This pattern of common and distinct regions suggests both shared and domain-specific neural underpinnings of mathematical and reading abilities.

Neurotransmitter mapping for reading ability

To identify the molecular substrates related to reading ability, we applied the same neurotransmitter mapping approach to the CCA-derived brain structural organization associated with reading. This parallel analysis allowed direct comparison of molecular substrates across cognitive domains while maintaining methodological consistency.

In the CMI-HBN discovery cohort, NMDA receptor distribution significantly mapped onto brain structural organization associated with reading ability (adjusted R^2 = 0.09, FDR-corrected spin-test p = 0.038, BF_{10} = 3.0e3). The spatial distribution of NMDA receptors was positively correlated with regions where greater grey matter volume predicted better reading performance (Fig. 8a).

In the Stanford validation cohort, NMDA receptor distribution again significantly mapped onto reading-related brain structural organization (adjusted R^2 = 0.08, FDR-corrected spin-test p = 0.009, BFr_{10} = 4.1). Several other neurotransmitter systems showed significant associations in this cohort (including $mGluR_5$, dopamine D_1, and acetylcholine $\alpha_4\beta_2$; Fig. 8b).

Notably, NMDA was the only neurotransmitter system that showed consistent relationships across both cohorts (Fig. 5b), as indicated by significant effects in both the discovery and validation samples. This cross-cohort consistency substantiates the role of glutamatergic signaling, particularly through NMDA receptors, in its association with brain structural organization supporting reading ability.

Network-level NMDA mapping for reading ability

Given NMDA's consistent relationship with reading ability across cohorts, we examined how these relationships manifested across different functional brain networks.

In the CMI-HBN discovery cohort, NMDA receptor distribution showed significant positive correlations with reading-related brain structural organization in two networks: dorsal default mode ($t(21) = 4.00$, r = 0.66, 95% CI [0.34, 0.84], FDR-corrected p = 0.008) and higher-order visual networks ($t(12) = 3.73$, r = 0.73, 95% CI [0.33, 0.91], FDR-corrected p = 0.019) (Fig. 6e; Supplementary Table 5).

In the Stanford validation cohort, the network-level relationships observed in the discovery cohort were replicated in the higher-order visual ($t(12) = 2.60$, $r = 0.60$, 95% CI [0.10, 0.86], FDR-corrected $p = 0.046$) but not the dorsal default mode network (Fig. 6e; Supplementary Table 5).

This more focused pattern, in contrast to the distributed network relationships observed for mathematical ability, suggests that NMDA receptor distribution relates to reading ability primarily through visual processing networks.

Stability of brain-behavior-receptor associations across age groups

Given that our neurotransmitter inferences necessarily relied on receptor maps derived from adults while our brain-behavior data came from children, we conducted comprehensive analyses to examine whether these associations were stable across age groups. Our results demonstrate that the brain-behavior-receptor associations identified above are stable across age groups and relate to the neurobiological underpinnings of math and reading skills (Supplementary Notes).

Disentangling shared and domain-specific contributions

To further parse shared versus domain-specific effects, we conducted a joint CCA including both math and reading measures simultaneously. We identified a shared academic-skill mode in both the CMI-HBN and Stanford cohorts, but did not observe a consistent and interpretable separation into math-specific and reading-specific modes. Neurotransmitter mapping of this shared mode

again highlighted NMDA as the only receptor showing consistent cross-cohort associations. Comparison of brain weight maps across models indicated that the original math- and reading-related modes are driven primarily by variance shared across mathematics and reading, while still retaining some domain-specific variance and therefore not being fully reducible to the shared component alone. This further suggests that NMDA receptor associations reflect primarily shared structural variance across both academic domains, while also capturing domain-relevant organization (See Supplementary Notes for details).

Discussion

Our study provides important insights into the molecular substrates supporting mathematical and reading abilities in children by comprehensively mapping neurotransmitter systems onto brain structural organization. Three key findings emerged from our analyses. First, NMDA receptor distribution consistently and robustly corresponded with brain structural organization associated with both mathematical and reading abilities across two independent cohorts, highlighting a critical association between glutamatergic signaling and cognitive development. Second, the spatial pattern of NMDA receptor associations differed across cognitive domains: associations were widely distributed across multiple functional networks for mathematical ability, whereas they were more focal within visual networks for reading ability, suggesting both common and domain-specific molecular substrates. Third, these associations showed notable specificity to NMDA receptors, while other neurotransmitter systems exhibited weaker, less consistent, or non-replicable relationships. Our findings establish a crucial bridge between molecular neurobiology and cognitive function, revealing how specific neurotransmitter systems relate to

the neural architecture underlying mathematical and reading abilities in the developing brain, and advance an integrative framework that spans from receptor-level organization to complex cognitive skills essential for academic achievement.

Prior neuroanatomical studies of mathematical and reading abilities have predominantly employed univariate voxel-based morphometry (VBM) approaches, testing each brain region independently [10,12,67-81]. CCA, by contrast, identifies the multivariate combination of brain regions whose grey matter volumes collectively covary most strongly with academic performance across individuals, yielding a distributed spatial phenotype that is then used as the basis for neurotransmitter mapping. This approach captures coordinated, brain-wide structural patterns that would be missed by region-by-region testing, and is particularly well-suited for linking to the spatially comprehensive PET-derived receptor maps. A detailed comparison of our findings with the prior VBM-based structural brain imaging literature, as well as discussion of convergent and divergent regional patterns of findings observed across cohorts, is provided in the Supplementary Discussion.

Our study is anchored in the well-established principle that excitatory-inhibitory (E/I) balance is fundamental to cognitive development and learning [38], with disruptions in this balance implicated in various neurodevelopmental disorders [30,82]. This framework, supported by extensive human and rodent research, posits that optimal learning requires precise coordination between glutamate-mediated excitation and GABA-mediated inhibition [31,38,64]. Given that academic skill acquisition involves intensive neural plasticity and circuit refinement during childhood, we hypothesized that glutamatergic and GABAergic receptor distributions would

show spatial correspondence with brain structural organization supporting mathematical and reading abilities.

Our findings specifically, and consistently, implicate NMDA receptor-mediated glutamatergic signaling as a key molecular substrate of both abilities. The robust and replicable spatial alignment between NMDA receptor density and structural phenotypes across independent cohorts suggest that regions where grey matter volume most strongly covaries with academic ability tend to be regions with higher NMDA receptor density, a pattern consistent with the view that NMDA receptor-dependent synaptic plasticity processes may contribute to experience-driven circuit refinement supporting learning and memory [24,28,83,84]. In contrast, the absence of consistent GABA associations across cohorts suggests a less dominant role for inhibitory signaling in these large-scale structural organization. Previous regional MRS studies have linked local GABA concentrations to mathematical skills in children [37] and in adolescents and young adults [46,47]. This pattern may suggest that GABAergic effects are more regionally specific and potentially more prominent at later developmental stages, whereas NMDA receptor distributions may play a more foundational role in the broader structural organization of academic skill networks during childhood (see Supplementary Discussion).

Our findings reveal both convergent and divergent neurochemical signatures across domains. For mathematical abilities, NMDA receptor density spatially corresponded with brain structural organization spanning insula, anterior cingulate, and prefrontal cortices, regions consistently implicated in numerical cognition and mathematical reasoning [8-10,68,70,72-74,76,77,79,80,85-88]. The prefrontal predominance of this pattern is consistent with anatomical evidence that layer 3

pyramidal neurons in prefrontal cortex have greater density of NMDA-dependent synaptic input than their parietal counterparts [89], and with the spatial distribution of NMDA receptor density in the Hansen et al. atlas itself [59] (see Supplementary Discussion).

For reading abilities, NMDA receptor density showed spatial correspondence with brain structural organization in prefrontal and, notably, ventral temporal-occipital cortex, a key region for orthographic processing and visual word recognition. These regions encompass both reading-specific and domain-general circuits implicated in attention and executive function, all critical for successful reading acquisition and proficiency [71,75,90-92]. These findings are consistent with the neuronal recycling hypothesis, which postulates that reading acquisition repurposes neural circuits, originally evolved for object recognition, toward processing written language [92]. The spatial correspondence between NMDA receptor density and grey matter volume associations with reading ability in ventral temporal-occipital cortex is consistent with the idea that NMDA receptor-dependent plasticity may facilitate the functional specialization of visual cortical neurons during reading acquisition [93,94].

Importantly, NMDA receptor associations for reading were more spatially constrained, concentrated within higher-order visual networks, compared to the multi-network pattern observed for mathematics, providing structural-level evidence for partially dissociable neurochemical substrates across domains despite their shared glutamatergic basis. While mathematical and reading abilities share substantial cognitive, genetic, and environmental architecture, evidenced by moderate-to-strong behavioral correlations across our cohorts (r = 0.39–0.57) and overlapping genetic risk factors [65,66], the domain-level differences in NMDA

spatial patterns suggest that common glutamatergic receptor architecture is expressed through partially distinct circuit-level organization for each skill.

Our whole-brain neurotransmitter mapping substantially extends previous regional MRS studies by moving beyond isolated brain areas and by examining replicability in independent cohorts [37,46-48,95]. A critical distinction from MRS-based approaches is that the present study uses population-level PET receptor density maps as a spatial reference, rather than directly measuring individual participants' neurochemical levels. These approaches are therefore complementary: PET-derived atlas maps provide spatially comprehensive, receptor-specific information that can contextualize and guide MRS research, while MRS provides individual-level neurochemical measurements within specific regions that can directly test mechanistic hypotheses suggested by atlas-based findings (see Supplementary Discussion for an integrative framework).

Beyond glutamate and GABA, our whole-brain mapping of 19 neurotransmitter receptors and transporters enabled examination of modulatory systems, including dopamine, serotonin, and acetylcholine, which are not readily accessible in traditional MRS studies. Despite theoretical predictions that these systems would show domain-general associations given their roles in reward-based learning, motivation, sustained attention, and cognitive flexibility [39-43], evidence for these systems was weaker and inconsistent across cohorts. While suggestive associations emerged, particularly for dopaminergic systems with mathematical abilities and cholinergic systems with reading abilities, these did not achieve cross-cohort replicability. These results suggest that modulatory neurotransmitter systems may influence academic skill acquisition

through more variable and indirect pathways, rather than being reflected in the stable structural organization of academic skill networks.

The present findings gain additional interpretive depth when considered alongside our prior transcriptomic work demonstrating that math-related brain structural organization is associated with genes enriched for voltage-gated potassium channel activity [86]. Potassium channels are essential for maintaining resting membrane potentials, controlling synaptic transmission, and shaping action potentials [96-99]. NMDA receptors and potassium channels are functionally coupled: NMDA receptor activation leads to calcium influx that activates calcium-dependent potassium channels, altering neuronal excitability and synaptic plasticity [100,101], while potassium channel activity regulates post-synaptic depolarization and thereby modulates the voltage-dependent magnesium block of NMDA receptors [102]. This bidirectional relationship creates a finely tuned system for regulating neural excitability and plasticity critical for learning and memory [28,30-38]. Anomalies in potassium channel-associated genes have been identified in individuals with learning disabilities [103] and neurodevelopmental delays [98], and disruptions in NMDA receptor-mediated signaling are similarly linked to learning impairments [104,105]. Together, our NMDA receptor and prior transcriptomic findings converge on a common neurobiological pathway involving the interplay between excitatory neurotransmission and membrane excitability, which may underlie the structural organization of circuits supporting academically-relevant cognitive abilities and offer promising targets for intervention and biomarker development.

Several limitations warrant consideration. First, our sample was restricted to children aged 7-14, excluding earlier developmental periods and later specialization phases. Although the CMI-HBN cohort extends to age 21, we intentionally restricted the age range to match the Stanford validation cohort. Examining an older CMI-HBN subgroup in future work would test developmental generalizability of the present effects. Second, our neurotransmitter inferences relied on receptor maps derived from over 1,200 healthy adults (mean ages 19.9-68.3 years) rather than age-matched children [59]. Neurotransmitter receptor systems undergo substantial developmental changes, including the protracted maturation of NMDA receptor subunit composition [106-108]. The adult-derived molecular maps may therefore not fully reflect the neurotransmitter landscape of the developing brain, and our interpretations regarding developmental plasticity mechanisms should be treated as theoretically motivated hypotheses rather than directly demonstrated conclusions. Our analyses confirm that brain-behavior-receptor associations are developmentally stable across the age range examined. Developing pediatric neurotransmitter atlases and novel non-invasive imaging methods with appropriate ethical safeguards, remains a priority albeit a challenging one. Third, the cross-sectional design precludes causal inference. Longitudinal designs tracking brain structure, academic abilities, and molecular markers across development, combined with intervention studies targeting neurotransmitter systems, would provide critical insights into developmental mechanisms. Finally, future studies employing larger samples with sufficient power to reliably characterize domain-specific structural phenotypes, as well as samples enriched for selective learning disabilities affecting only one domain, will be essential for determining whether glutamatergic signaling relates differentially to mathematical versus reading abilities or whether it constitutes a common neurobiological substrate underlying academic skill acquisition more broadly.

In summary, our study provides a comprehensive brain-wide mapping of neurotransmitter receptor distributions that spatially correspond to the structural organization of networks supporting children's academic abilities. Across 19 neurotransmitter receptors and transporters examined, NMDA receptor distribution showed robust and spatially selective associations with brain structural organization for both mathematical and reading abilities across two independent cohorts, highlighting the specific and replicable role of NMDA receptor-mediated glutamatergic signaling in academic skill development. By bridging molecular neuroscience and cognitive development, our findings offer an integrated multi-level framework for characterizing individual differences in academic abilities. Future studies integrating molecular, neural, and behavioral assessments across developmental stages will be essential for translating these insights into effective educational and clinical strategies.

Methods

Participants

CMI-HBN discovery cohort. The Child Mind Institute – Healthy Brain Network (CMI-HBN) is an open resource for transdiagnostic research in pediatric mental health and learning disorders [63]. Given its large sample size and wide age range, we used it as our discovery cohort. Our initial sample comprised 1,236 typically developing children aged 7 to 14 years with Full Scale IQ scores of 80 or above on the WISC-V [109] and valid scores of numerical operations, math problem-solving, word reading, and reading comprehension subtests of the WIAT-III [110]. Among

these children, 858 had structural MRI images collected within one year of WIAT-III score collection. These scans underwent a multistage quality control procedure (see Quality Control for details), including manual review of raw structural images and visual inspection of post-processing outputs following processing with the Advanced Normalization Tools (ANTs) pipeline [111]. Based on these quality control procedures, 98 children were excluded because of poor image quality and/or unsatisfactory processing outputs. The remaining scans were retained for grey matter volume computation. Consequently, the final cohort for further analysis consisted of 760 children, including 485 males and 275 females (Table 1).

Stanford validation cohort. We pooled data across multiple research studies conducted at Stanford University. Informed written consent was obtained from the child's legal guardian and the protocol was approved by the Stanford University Institutional Review Board for the original studies. Our initial sample comprised 423 typically developing children aged 7 to 14 years with Full Scale IQ scores of 80 or above on the WASI-I/II [112] and valid scores of numerical operations, math reasoning, word reading, and reading comprehension subtests of the WIAT-II [113]. Among these children, 240 had structural MRI images collected within one year of WIAT-II score collection. These scans underwent a multistage quality control procedure (see Quality Control for details), including manual review of raw structural images and visual inspection of post-processing outputs following processing with the ANTs pipeline [111]. Based on these quality control procedures, 9 children were excluded because of poor image quality and/or unsatisfactory processing outputs. The remaining scans were retained for grey matter volume computation. Consequently, the final cohort for further analysis consisted of 231 children, including 133 males and 98 females (Table 1).

Sex reporting. Sex information was obtained from the demographic variables provided by each cohort. In the CMI-HBN cohort, participants were categorized as male or female based on the demographic information available in the public dataset. In the Stanford cohort, participants were categorized as male or female based on demographic information collected as part of the original study protocol. Sex was considered in sample characterization and is reported for each cohort. The present study was designed to identify brain structural phenotypes associated with mathematical and reading abilities and to test their correspondence with neurotransmitter receptor maps across independent cohorts. To examine whether the identified brain-behavior relationships were present in both male and female participants, sex-stratified analyses were conducted in both cohorts (see Supplementary Notes).

Ethics and informed consent

For the CMI-HBN cohort, data were obtained from the publicly available Child Mind Institute Healthy Brain Network (CMI-HBN) database. All participants provided informed consent (or assent with parental/guardian consent) under protocols approved by the institutional review boards overseeing data collection by the original investigators. Information on participant compensation for the CMI-HBN cohort was determined by the original study protocols and was not available to the present study investigators.

For the Stanford cohort, all participants (and their legal guardians for minors) provided written informed consent in accordance with protocols approved by the Stanford University Institutional Review Board (IRB Protocol No. 11849 and Assurance No. FWA00000935 (SU)). Participant

compensation, if applicable, was administered according to the approved Stanford study protocol.

Standardized assessments of math and reading abilities

We used subtests from the WIAT-II/III neuropsychological assessment [110,113] to measure children's math and reading abilities. Grade-normed standardized scores were used to minimize potential differences between different versions of equivalent subtests.

CMI-HBN discovery cohort. Standardized scores of numerical operations and math problem solving subtests from the WIAT-III were used to measure children's math abilities; standardized scores of word reading and reading comprehension subtests from the WIAT-III were used to measure children's reading abilities.

Stanford validation cohort Standardized scores of numerical operations and math reasoning subtests from the WIAT-II were used to measure children's math abilities; standardized scores of word reading and reading comprehension subtests from the WIAT-II were used to measure children's reading abilities.

The numerical operations subtest (WIAT-II/III) evaluates children's ability to identify and write dictated numerals and solve written calculation problems and equations involving addition, subtraction, multiplication, and division. The math reasoning (WIAT-II) and math problem solving (WIAT-III) subtests evaluate children's ability to use math reasoning and problem-

solving skills, including identification of geometric shapes and single- and multi-step word problems involving time, money, and measurement. The word reading subtest (WIAT-II/III) evaluates children's ability to read familiar words aloud from a list. The reading comprehension subtest (WIAT-II/III) requires children to match a written word with its representative picture, read different types of passages, and respond to questions involving comprehension of the content.

Structural MRI data acquisition

CMI-HBN discovery cohort. The CMI-HBN is an open resource dataset for transdiagnostic research in pediatric mental health and learning disorders [63]. MRI images were acquired at multiple sites with protocols and parameters varied across locations. Details of CMI-HBN imaging protocols can be found at the data portal website: https://fcon_1000.projects.nitrc.org/indi/cmi_healthy_brain_network/MRI_Protocol.html.

Stanford validation cohort. Structural MRI images were acquired at Stanford University Lucas Center on a 3T GE scanner (General Electric, Milwaukee, WI). Head movement was minimized using additional pads and pillows around children's heads. Image parameters are listed in Supplementary Table 6.

Quality Control

The structural MRI data underwent a multistage, manual, and systematic quality control procedure prior to inclusion in the final analyses. For each participant and visit, all available T1-weighted scans were first visually reviewed to identify the optimal acquisition. Raw-image inspection focused on artifacts including ringing, ghosting, blurring, susceptibility-related signal loss, radiofrequency noise/spiking, intensity inhomogeneity, wrapping artifacts, and field-of-view clipping. When multiple scans were available, the highest-quality scan was selected for processing. The selected scans were then processed using the ANTs pipeline. Post-processing quality control included visual inspection of brain extraction, tissue segmentation, and downstream outputs. QC reports displaying extracted brain images and grey matter/white matter segmentations overlaid on the native anatomy in axial, coronal, and sagittal views were reviewed to assess tissue classification accuracy, boundary integrity, and over- or under-extraction. Downstream outputs were additionally inspected for anatomical plausibility, focal outliers, boundary irregularities, and consistency with the underlying anatomy. Structural scans were rated on a 0–5 scale, where 0 indicated unusable data, 1 poor quality unusable for research, 2 fair quality with substantial artifacts and likely unusable, 3 good quality with some artifacts that did not preclude interpretation, 4 very good quality with only minor artifacts, and 5 excellent quality with no discernible artifacts. Ratings were performed independently by two raters, and discrepant cases were resolved by detailed review and consensus discussion. Scans flagged as problematic at any stage underwent further review to determine whether reprocessing, substitution with an alternative scan from the same visit, adjustment of brain extraction parameters, or exclusion was warranted.

Estimation of grey matter volume

To estimate the grey matter volume for each child, we used the volume-based Advanced Normalization Tools (ANTs v2.3.5) Longitudinal Cortical Thickness Pipeline (LCT) [111], which comprises well-vetted components for multivariate template construction, image registration, bias correction, n-tissue segmentation, and cortical thickness estimation.

First, we created a population-specific template from 259 quality controlled T1-weighted structural images of a pediatric population aged 7-14 years collected at Stanford University. Among the T1-weighted images, 59 of them overlapped with our final sample of the Stanford validation cohort. This template was generated using the ANTs multivariate template construction component, which mapped the images to a common anatomy and iteratively estimated the average shape and appearance image.

Second, we utilized ANTs Atropos component and the publicly available Oasis template tissue priors [114] to segment the population specific template into 6 tissue classes, including cerebrospinal fluid (CSF), grey matter (GM), white matter (WM), deep grey matter (striatum and thalamus), brain stem, and cerebellum. The tissue probability maps of the 6 tissue classes were further generated for the population specific template using ANTs cook component, which were then used to generate for each child a single subject template (SST) that proceeds through the ANTs cross-sectional Cortical Thickness Pipeline producing a brain extraction mask and a CSF tissue probability map in the SST space. Joint label fusion was further performed to create tissue probability maps for all 6 tissue classes for each child.

Third, we used the ANTs LCT Pipeline to generate cortical thickness maps for each child. This process involves the creation of a SST for each child using all available images collected at multiple time points, the population specific template and its priors that were generated from the step above as a reference. This process generates individualized probability maps for all 6 tissue classes and cortical thickness estimation in the SST space. The SST and resulting tissue priors are warped into individual subject space and serve as the reference template for processing of each structural MRI image. Individual-level n4 bias correction, brain extraction, and tissue segmentations are generated prior to cortical thickness estimation. Cortical Thickness (CT) is estimated using the Diffeomorphic Registration-based Estimation algorithm (DiReCT), which involves the alignment of the white matter (WM) probability map to the combined grey matter/white matter (GM/WM) probability maps. This process allows for assignment of cortical thickness values to each spatial location within the cortex, following a diffeomorphic path at each GM/WM interface until the grey matter/cerebrospinal fluid (GM/CSF) boundary is reached. CT and tissue segmentation quality was assessed to ensure integrity of brain extractions, segmentation, spatial normalization, and cortical thickness estimates.

Finally, each individual's SST generated from the LCT pipeline allows for the computation of grey matter volume. Each child's brain is registered to the Brainnetome atlas in the SST space, ensuring consistent anatomical comparisons across individuals. The high-resolution (1mm isotropic) ROIs provided by the atlas serve as precise references for defining specific brain regions. After registration, a binarized mask is created for each ROI to isolate grey matter from the cortical thickness LCT output images. Using this mask in combination with cortical thickness outputs allows for the calculation of cortical thickness, surface area, and grey matter volume

estimates within each ROI. Because subcortical structures such as basal ganglia lack the distinct grey-white and grey-CSF boundaries required for cortical thickness estimation, the LCT pipeline treats these regions as tissue priors. Consequently, we included only the first 218 Brainnetome ROIs for analysis, excluding ROIs 219-246 that corresponds to the subcortical prior regions. In the current study, we focused on grey matter volume only.

Canonical correlation analysis

We conducted canonical correlation analysis (CCA), a powerful multivariate method for capturing associations between 2 modalities of data (e.g., brain and behavior), to determine the multivariate associations between mathematical or reading abilities and brain structure organization. Prior to analysis, extreme outliers were identified for each brain and behavioral variable of interest using an interquartile range (IQR-based rule). Specifically, extreme outliers were defined as observations more than three interquartile ranges below the first quartile or above the third quartile. Participants identified as extreme outliers on any variable were excluded from further analyses. This resulted in the removal of 9 participants from the CMI-HBN cohort and 3 participants from the Stanford cohort, yielding final CCA samples of 751 participants for CMI-HBN and 228 participants for Stanford.

CMI-HBN discovery cohort. Two standardized scores including numerical operations and math problem-solving scores from the WIAT-III were used to capture associations between math abilities and grey matter volume, and two standardized scores including word reading and reading comprehension scores from the WIAT-III were used to capture associations between

reading abilities and grey matter volume. Given the moderate correlations between math or reading abilities and age (see Supplementary Notes), we controlled for age in the analyses of brain-behavior relationships by including age together with the math or reading ability measures as the behavioral variable set (**Y**). Moreover, grey matter volume of the 218 brain regions of interest from the Brainnetome atlas [115] were used as the brain variable set. To avoid overfitting and multicollinearity issues, we reduced the dimensionality of the brain variable set (**X**) by applying a principal component analysis (PCA) and retained the first 17 components that together explained 90% of the total variance. The behavior variable set and the retained principal components ($\mathbf{X}_{pca}$) of the brain variable set were subsequently fed into CCA.

CCA takes the brain and behavioral variable sets $\mathbf{X}_{pca}$ and **Y** as inputs and identifies pairs of brain and behavioral weights **A** and **B** such that the linear combination (weighted sum) of the brain and behavioral variables maximizes the correlation between the resulting brain and behavioral canonical variates, i.e. $\mathbf{U} = \mathbf{X}_{pca}\mathbf{A}$ and $\mathbf{V} = \mathbf{YB}$. A canonical mode refers to a pair of canonical variates that jointly share variance in both variables sets. The canonical correlation of a mode refers to the Pearson correlation between its corresponding pair of canonical variates.

A permutation test was performed to assess the significance of CCA model fit and canonical modes. Specifically, for CCA involving math ability measures, we permuted the order of numerical operations and math problem-solving scores in the behavioral variable set; for CCA involving reading ability measures, we permuted the order of word reading and reading comprehension scores in the behavioral variable set. Next, we re-ran CCA using the permuted behavioral variable set ($\mathbf{Y}_{perm}$) and the original brain variable set ($\mathbf{X}_{pca}$), and recorded the model

fit as well as canonical correlation for each mode. This procedure was repeated for 5,000 times for each CCA model, and the recorded model fits and canonical correlations were used to establish their null distributions. The observed model fit, quantified using Pillai's trace, and the canonical correlations were compared with their respective null distributions to determine permutation *p* values. Permutation *p* values were computed as the proportion of permuted statistics greater than or equal to the observed statistic. FDR correction was applied where appropriate.

Finally, to obtain relative weights and signs of involvement of the original brain and behavioral variables, we correlated **U** and **V** respectively against the original brain (**X**) and behavioral (**Y**) variables. We focused on modes that survived permutation tests, and interpreted their meanings according to the relative weights of behavioral variables. The relative weights of brain variables were further used to explore the mapping between neurotransmitter systems and brain structure organizations associated with math and reading abilities.

***Stanford validation cohort*.** To examine the replicability of our findings, we applied the same CCA procedure to determine the multivariate associations between mathematical or reading abilities and brain structure organization in an independent Stanford validation cohort.

Briefly, two standardized scores including numerical operations and math reasoning scores from the WIAT-II were used to capture associations between math abilities and grey matter volume, and two standardized scores including word reading and reading comprehension scores from the WIAT-II were used to capture associations between reading abilities and grey matter volume.

Given the moderate correlations between math or reading abilities and age (see Supplementary Notes), we controlled for age in the analyses of brain-behavior relationships by including age together with the math or reading ability measures as the behavioral variable set (**Y**), and grey matter volume of the 218 brain regions of interest from the Brainnetome atlas [115] as the brain variable set. We reduced the dimensionality of the brain variable set (**X**) by applying a PCA and retained the first 13 components that together explained 90% of the total variance. The behavior variable set and the retained principal components ($\mathbf{X}_{pca}$) were subsequently fed into CCA. The significance of CCA model fit and canonical modes were assessed using permutation tests with 5,000 iterations. Finally, we obtained the relative weights and signs of involvement of the original brain and behavioral variable, and used them to interpret the meanings of significant canonical modes and explore the mapping between neurotransmitter systems and brain structure organizations associated with math and reading abilities.

For visualization, the signs of the canonical variates and corresponding loadings were oriented so that higher behavioral canonical scores correspond to higher academic performance; this sign orientation does not affect canonical correlations or statistical significance.

Out-of-sample generalization of brain-behavior relationships

To directly examine the generalizability of the brain-behavior findings, we applied the CCA model derived from the CMI-HBN discovery cohort to an independent Stanford validation cohort, and assessed the correlation between the predicted brain and behavioral canonical variates.

On the behavioral side, the analysis of math abilities used age and two standardized scores – numerical operations and math problem-solving scores from the WIAT-II in the Stanford validation cohort – as the behavioral variable set ($\mathbf{Y}_{\text{Stanford}}$). Similarly, the analysis of reading abilities used age and two standardized scores – word reading and reading comprehension scores from the WIAT-II in the validation cohort – as the behavioral variable set ($\mathbf{Y}_{\text{Stanford}}$).

On the brain side, we projected the grey matter volumes of 218 regions of interest from the Stanford validation cohort onto the same dimensional space as the CMI-HBN discovery cohort. This process involved centering the brain variables of the validation cohort using the mean values from the discovery cohort, and then applying the PCA rotation matrix derived from the discovery cohort to the centered data. Finally, we retained the first 17 principal components, aligning with the discovery cohort's dimensionality. This resulting brain variable set for the Stanford validation cohort is referred to as $\mathbf{X}_{\text{pca-Stanford}}$.

We then computed the predicted brain canonical variates ($\mathbf{U}_{\text{Stanford}}$) by multiplying the brain variable set, $\mathbf{X}_{\text{pca-Stanford}}$, by the brain weights $\mathbf{A}$ derived from the CMI-HBN discovery cohort. Similarly, we obtained the predicted behavioral canonical variates ($\mathbf{V}_{\text{Stanford}}$) by multiplying the behavioral variable set, $\mathbf{Y}_{\text{Stanford}}$, by the behavioral weights $\mathbf{B}$ derived from the CMI-HBN discovery cohort. We then computed the Pearson correlations between the predicted brain and behavioral canonical variates for the mathematics- and reading-related modes in the validation cohort. To evaluate the significance of the predicted canonical correlation, we permuted the predicted behavioral canonical variate and computed its Pearson correlation with the predicted

brain canonical variate. This permutation procedure was repeated 5,000 times to generate a null distribution, which was then used to assess the significance of the observed predicted canonical correlation. Upper-tail permutation *p* values were computed as the proportion of permuted correlations greater than or equal to the observed correlation. For visualization, the signs of the predicted brain and behavioral canonical variates were oriented so that higher grey matter volume scores correspond to higher academic performance; this sign orientation does not affect canonical correlations or statistical significance.

Maps of neurotransmitter receptors and transporters

We used the volumetric PET images (https://github.com/netneurolab/hansen_receptors/tree/main/data/PET_nifti_images/) shared by Hansen et al. [59] to derive the whole-brain maps of the 19 neurotransmitter receptors and transporters (Supplementary Fig. 2). Specifically, these PET images were collected from over 1,200 healthy participants across multiple studies and averaged across individual participant maps within studies shared before [59]. The images are an estimate proportional to receptor densities. We registered the images to the MNI 152 template and then parcellated into 246 brain regions according to the brainnetome atlas. Receptors and transporters with more than one mean image of the same tracer (e.g., D_2, $mGluR_5$) were combined using a weighted average. Finally, each receptor/transporter map was z-scored across regions for further analysis.

Neurotransmitter mapping of brain organization for math and reading

We further investigated how the spatial distributions of neurotransmitter systems correspond to brain structural organization associated with mathematical or reading ability.

CMI-HBN discovery cohort. We examined 19 neurotransmitter receptors and transporters [59] to test the hypothesis that glutamate ($mGluR_5$, NMDA), the primary excitatory neurotransmitter, and GABA ($GABA_{A/BZ}$), the main inhibitory neurotransmitter, would map onto variation in brain structural organization associated with math or reading ability. For each neurotransmitter receptor or transporter, we fitted a linear regression model with the whole-brain neurotransmitter map as the independent variable and the CCA-derived brain weight map associated with math or reading ability as the dependent variable. Model significance was assessed using spatial autocorrelation-preserving spin-permuted tests with 5,000 iterations (see Null Model section). Permutation *p* values were computed using upper-tail tests by comparing the observed model fit with the null distribution generated from spin-permuted maps. Multiple comparisons across neurotransmitter maps were controlled using the false discovery rate (FDR) approach.

Additionally, we computed Bayes factors (BF_{10}) to quantify the strength of evidence for each neurotransmitter model relative to an intercept-only null model in the CMI-HBN discovery cohort. Bayes factors were computed using the lmBF function in the R BayesFactor package. We used the default Jeffreys-Zellner-Siow prior specification for Bayesian linear models and the default medium Cauchy prior scale for standardized regression coefficients. No Markov chain Monte Carlo sampling was used, as lmBF computes Bayes factors by numerical integration. Individual neurotransmitter receptors or transporters were considered as significant if both the FDR-corrected spin-test *p* value was < 0.05 and BF_{10} was > 3.

Stanford validation cohort. To examine replicability of our findings, we conducted the same neurotransmitter mapping analysis in the independent Stanford validation cohort. For the Stanford cohort, we additionally computed replication Bayes Factor (BFr_{10}) to quantify the strength of evidence from the Stanford validation cohort given data already acquired from the CMI-HBN discovery cohort [116]. For each neurotransmitter map, BFr_{10} was calculated as the Bayes factor from the combined CMI-HBN and Stanford datasets divided by the Bayes factor for the CMI-HBN discovery dataset alone. Thus, BFr_{10} quantified the additional evidence for the association provided by the Stanford validation cohort. Bayes factors for the discovery, validation, and combined datasets were computed using the same lmBF model specification, default Jeffreys-Zellner-Siow prior, and default medium Cauchy prior scale described above. No Markov chain Monte Carlo sampling was used. Individual neurotransmitter receptors or transporters were considered as significant if both FDR-corrected spin-test p value was < 0.05 and BFr_{10} was > 3.

Network-level neurotransmitter mapping for math and reading

For neurotransmitter receptors consistently showing significant association with brain structural organization supporting mathematical or reading ability across cohorts, we further conducted network-level analysis to examine how these relationships manifested across different functional brain networks.

CMI-HBN discovery cohort. For each Brainnetome ROI, we calculated the number of overlapping voxels between the ROI and each of the 14 Shirer network [117], assigning the ROI to the network with the greatest overlap. Next, for each Shirer network, we examined the correlation between the distribution of a receptor and the CCA-derived brain weight map associated with mathematical or reading ability.

Stanford validation cohort. We examined the replicability of our findings using the same network-level analysis, focusing on networks showing significant effects in the discovery cohort.

Significance was assessed using two-sided Pearson correlations across ROIs within each Shirer network. The number of ROIs varied across networks and results from networks with small numbers of ROIs should be interpreted cautiously.

Null Models

To assess the statistical significance of associations across brain regions, we employed spatial autocorrelation-preserving permutation tests (spin tests). Specifically, we utilized the Moran spectral randomization method [118] as implemented in the BrainSpace Python package (https://brainspace.readthedocs.io/). This method generates surrogate brain maps with spatial autocorrelation that matches the spatial autocorrelation observed in the original brain-behavior association map. This procedure involves constructing a spatially-informed weight matrix, typically represented as an inverse distance matrix between brain regions. An eigen decomposition of this matrix is then performed to derive spatial eigenvectors, which estimate the

autocorrelation structure. These eigenvectors are subsequently used to impose a similar spatial structure on randomly generated surrogate data.

For each spin test, we generated 5,000 null maps based on the original brain weight map obtained from CCA. Linear regressions were conducted to map neurotransmitter systems onto each of the 5,000 null maps, resulting in a distribution of 5,000 adjusted R^2 values. This null distribution was then used to assess the significance of the observed adjusted R^2 value from the original data by comparing it against the corresponding null distribution.

Software and packages

Analyses and figure generation were performed using R v4.3.1, Python v3.11.13, and MATLAB R2023a. Structural MRI processing was performed using Advanced Normalization Tools (ANTs v2.3.4). R analyses used the packages CCA, CCP, ppcor, BayesFactor, permute, psych, readxl, R.matlab, reshape2, ggplot2, ggrepel, and ggseg. Python analyses used numpy, pandas, scipy, scikit-learn, and BrainSpace. Matlab-based visualization of brain maps was performed using BrainNet Viewer (v1.7). Full package versions are provided in the code repository. Figures were assembled in Adobe Illustrator.

Data availability

The de-identified behavioral data and extracted grey matter volume values generated in this study and necessary to reproduce the study findings have been deposited in an archived GitHub repository release on Zenodo and are publicly available at https://doi.org/10.5281/zenodo.20574388 [119]. Source data generated in this study are provided

with this paper as a Source Data file. Raw imaging data from the CMI-HBN cohort used in this study are available through the Child Mind Institute Healthy Brain Network data portal at https://data.healthybrainnetwork.org/main.php, in accordance with the cohort's data access procedures and data use terms. Raw imaging data from the Stanford cohort are available under restricted access because the conditions of the ethics approval do not permit public archival or unrestricted public sharing of these data. Access to Stanford raw imaging data can be requested by contacting the corresponding authors and requires execution of a Data Use Agreement with Stanford University. Access is subject to approval by Stanford University and is limited to research purposes consistent with the original ethics approval and participant consent. Requests will be reviewed in accordance with Stanford University policies. The atlas of PET-derived whole-brain neurotransmitter receptor maps used in this study, comprising 19 neurotransmitter receptors, receptor-binding sites, and transporters across nine neurotransmitter systems and more than 1,200 healthy individuals, is available at https://github.com/netneurolab/hansen_receptors.

Code availability

Custom code for analyses and visualization has been deposited in an archived GitHub repository release on Zenodo and is publicly available at https://doi.org/10.5281/zenodo.20574388 [119].

References

1 Ritchie, S. J. & Bates, T. C. Enduring links from childhood mathematics and reading achievement to adult socioeconomic status. *Psychol Sci* **24**, 1301-1308, doi:10.1177/0956797612466268 (2013).

2 Torre, G. A., Matejko, A. A. & Eden, G. F. The relationship between brain structure and proficiency in reading and mathematics in children, adolescents, and emerging adults. *Dev Cogn Neurosci* **45**, 100856, doi:10.1016/j.dcn.2020.100856 (2020).

3 OECD. *PISA 2018 Results*. (OECD Publishing, 2020).

4 Horowitz, S. H., Rawe, J. & Whittaker, M. C. *The state of learning disabilities: Understanding the 1 in 5*, 2017).

5 Ashkenazi, S. S. *et al.* Are Numerical Abilities Determined at Early Age? A Brain Morphology Study in Children and Adolescents with and without Developmental Dyscalculia. *Developmental Cognitive Neuroscience*, doi:10.1016/j.dcn.2024.101369 (2024).

6 Menon, V. & Chang, H. Emerging neurodevelopmental perspectives on mathematical learning. *Dev Rev* **60**, doi:10.1016/j.dr.2021.100964 (2021).

7 Menon, V., Padmanabhan, A. & Schwartz, F. Cognitive neuroscience of dyscalculia and math learning disabilities. (2020).

8 Popescu, T. *et al.* The brain-structural correlates of mathematical expertise. *Cortex* **114**, 140-150, doi:10.1016/j.cortex.2018.10.009 (2019).

9 Skeide, M. A. *et al.* Neurobiological origins of individual differences in mathematical ability. *PLoS Biol* **18**, e3000871, doi:10.1371/journal.pbio.3000871 (2020).

10 Wilkey, E. D., Cutting, L. E. & Price, G. R. Neuroanatomical correlates of performance in a state-wide test of math achievement. *Dev Sci* **21**, doi:10.1111/desc.12545 (2018).

11 Xiao, J. *et al.* Personalized Theta Burst Stimulation Enhances Social Skills in Young Minimally Verbal Children With Autism: A Double-Blind Randomized Controlled Trial. *Biol Psychiatry*, doi:10.1016/j.biopsych.2025.01.002 (2025).

12 He, Q. *et al.* Decoding the neuroanatomical basis of reading ability: a multivoxel morphometric study. *J Neurosci* **33**, 12835-12843, doi:10.1523/JNEUROSCI.0449-13.2013 (2013).

13 Lawn, T. *et al.* From neurotransmitters to networks: Transcending organisational hierarchies with molecular-informed functional imaging. *Neurosci Biobehav Rev* **150**, 105193, doi:10.1016/j.neubiorev.2023.105193 (2023).

14 Zacharopoulos, G., Dehghani, M., Krause-Sorio, B., Near, J. & Cohen Kadosh, R. Functional connectivity and GABAergic signaling modulate the enhancement effect of neurostimulation on mathematical learning. *PLoS biology* **23**, e3003200 (2025).

15 Hansen, J. Y. *et al.* Correspondence between gene expression and neurotransmitter receptor and transporter density in the human brain. *Neuroimage* **264**, 119671, doi:10.1016/j.neuroimage.2022.119671 (2022).

16 Ji, G.-J. *et al.* White matter dysfunction in psychiatric disorders is associated with neurotransmitter and genetic profiles. *Nature Mental Health* **1**, 655-666, doi:10.1038/s44220-023-00111-2 (2023).

17 Zhao, L. *et al.* Relationships between neurotransmitter receptor densities and expression levels of their corresponding genes in the human hippocampus. *Neuroimage* **273**, 120095, doi:10.1016/j.neuroimage.2023.120095 (2023).

18 Lujan, R., Shigemoto, R. & Lopez-Bendito, G. Glutamate and GABA receptor signalling in the developing brain. *Neuroscience* **130**, 567-580, doi:10.1016/j.neuroscience.2004.09.042 (2005).
19 Barkus, C. *et al.* Hippocampal NMDA receptors and anxiety: at the interface between cognition and emotion. *Eur J Pharmacol* **626**, 49-56, doi:10.1016/j.ejphar.2009.10.014 (2010).
20 Collingridge, G. The role of NMDA receptors in learning and memory. *Nature* **330**, 604-605 (1987).
21 Ghosh, A. Learning More About NMDA Receptor Regulation. *Science* **295**, 449–451 (2002).
22 Lee, I. & Kesner, R. P. Differential contribution of NMDA receptors in hippocampal subregions to spatial working memory. *Nat Neurosci* **5**, 162-168, doi:10.1038/nn790 (2002).
23 Kumar, A. NMDA Receptor Function During Senescence: Implication on Cognitive Performance. *Front Neurosci* **9**, 473, doi:10.3389/fnins.2015.00473 (2015).
24 Lisman, J. E., Fellous, J.-M. & Wang, X.-J. A role for NMDA-receptor channels in working memory. *Nature Neuroscience* **1**, 273-275 (1998).
25 Warburton, E. C., Barker, G. R. & Brown, M. W. Investigations into the involvement of NMDA mechanisms in recognition memory. *Neuropharmacology* **74**, 41-47, doi:10.1016/j.neuropharm.2013.04.013 (2013).
26 Castro-Alamancos, M. A., Donoghue, J. P. & Connors, B. W. Different Forms of Synaptic Plasticity in Somatosensory and Motor Areas of the Neocortex
. *The Journal of Neuroscience* **15**, 5324-5333 (1995).
27 Trepel, C. & Racine, R. J. GABAergic modulation of neocortical long-term potentiation in the freely moving rat. *Synapse* **35**, 120-128, doi:10.1002/(sici)1098-2396(200002)35:2<120::Aid-syn4>3.0.Co;2-6 (2000).
28 Pagano, J., Giona, F., Beretta, S., Verpelli, C. & Sala, C. N-methyl-d-aspartate receptor function in neuronal and synaptic development and signaling. *Curr Opin Pharmacol* **56**, 93-101, doi:10.1016/j.coph.2020.12.006 (2021).
29 Tang, X., Jaenisch, R. & Sur, M. The role of GABAergic signalling in neurodevelopmental disorders. *Nat Rev Neurosci* **22**, 290-307, doi:10.1038/s41583-021-00443-x (2021).
30 Ahmad, J. *et al.* From mechanisms to markers: novel noninvasive EEG proxy markers of the neural excitation and inhibition system in humans. *Transl Psychiatry* **12**, 467, doi:10.1038/s41398-022-02218-z (2022).
31 Dorrn, A. L., Yuan, K., Barker, A. J., Schreiner, C. E. & Froemke, R. C. Developmental sensory experience balances cortical excitation and inhibition. *Nature* **465**, 932-936, doi:10.1038/nature09119 (2010).
32 Nishiyama, M., Togashi, K., Aihara, T. & Hong, K. GABAergic activities control spike timing- and frequency-dependent long-term depression at hippocampal excitatory synapses. *Front Synaptic Neurosci* **2**, 22, doi:10.3389/fnsyn.2010.00022 (2010).
33 Shibata, K. *et al.* Overlearning hyperstabilizes a skill by rapidly making neurochemical processing inhibitory-dominant. *Nat Neurosci* **20**, 470-475, doi:10.1038/nn.4490 (2017).
34 Barron, H. C. *et al.* Unmasking Latent Inhibitory Connections in Human Cortex to Reveal Dormant Cortical Memories. *Neuron* **90**, 191-203, doi:10.1016/j.neuron.2016.02.031 (2016).

35 Wijtenburg, S. A. *et al.* Glutamatergic metabolites are associated with visual plasticity in humans. *Neurosci Lett* **644**, 30-36, doi:10.1016/j.neulet.2017.02.020 (2017).

36 Zacharopoulos, G., Emir, U. & Cohen Kadosh, R. The cross-sectional interplay between neurochemical profile and brain connectivity. *Hum Brain Mapp* **42**, 2722-2733, doi:10.1002/hbm.25396 (2021).

37 Zacharopoulos, G. *et al.* Predicting learning and achievement using GABA and glutamate concentrations in human development. *PLoS Biol* **19**, e3001325, doi:10.1371/journal.pbio.3001325 (2021).

38 van Bueren, N. E. R., van der Ven, S. H. G., Hochman, S., Sella, F. & Cohen Kadosh, R. Human neuronal excitation/inhibition balance explains and predicts neurostimulation induced learning benefits. *PLoS Biol* **21**, e3002193, doi:10.1371/journal.pbio.3002193 (2023).

39 Bech, P. *et al.* Striatal Dopamine Signals and Reward Learning. *Function (Oxf)* **4**, zqad056, doi:10.1093/function/zqad056 (2023).

40 Kehagia, A. A., Murray, G. K. & Robbins, T. W. Learning and cognitive flexibility: frontostriatal function and monoaminergic modulation. *Current opinion in neurobiology* **20**, 199-204 (2010).

41 Klanker, M., Feenstra, M. & Denys, D. Dopaminergic control of cognitive flexibility in humans and animals. *Frontiers in neuroscience* **7**, 201 (2013).

42 Logue, S. F. & Gould, T. J. The neural and genetic basis of executive function: attention, cognitive flexibility, and response inhibition. *Pharmacology Biochemistry and Behavior* **123**, 45-54 (2014).

43 Luo, Q. *et al.* Comparable roles for serotonin in rats and humans for computations underlying flexible decision-making. *Neuropsychopharmacology* **49**, 600-608, doi:10.1038/s41386-023-01762-6 (2024).

44 Visibelli, E., Vigna, G., Nascimben, C. & Benavides-Varela, S. Neurobiology of numerical learning. *Neurosci Biobehav Rev* **158**, 105545, doi:10.1016/j.neubiorev.2024.105545 (2024).

45 Ramus, F., Altarelli, I., Jednorog, K., Zhao, J. & Scotto di Covella, L. Neuroanatomy of developmental dyslexia: Pitfalls and promise. *Neurosci Biobehav Rev* **84**, 434-452, doi:10.1016/j.neubiorev.2017.08.001 (2018).

46 Zacharopoulos, G., Sella, F. & Cohen Kadosh, R. The impact of a lack of mathematical education on brain development and future attainment. *Proc Natl Acad Sci U S A* **118**, doi:10.1073/pnas.2013155118 (2021).

47 Zacharopoulos, G., Sella, F., Emir, U. & Cohen Kadosh, R. The relation between parietal GABA concentration and numerical skills. *Sci Rep* **11**, 17656, doi:10.1038/s41598-021-95370-3 (2021).

48 Pugh, K. R. *et al.* Glutamate and choline levels predict individual differences in reading ability in emergent readers. *J Neurosci* **34**, 4082-4089, doi:10.1523/JNEUROSCI.3907-13.2014 (2014).

49 Lebel, C., MacMaster, F. P. & Dewey, D. Brain metabolite levels and language abilities in preschool children. *Brain Behav* **6**, e00547, doi:10.1002/brb3.547 (2016).

50 Cecil, K. M., Brunst, K. J. & Horowitz-Kraus, T. Greater reading gain following intervention is associated with low magnetic resonance spectroscopy derived concentrations in the anterior cingulate cortex in children with dyslexia. *Brain Research* **1759**, doi:10.1016/j.brainres.2021.147386 (2021).

51 Ding, X.-Q. & Lanfermann, H. Whole brain 1H-Spectroscopy: a developing technique for advanced analysis of cerebral metabolism. *Clinical neuroradiology* **25**, 245-250 (2015).

52 Rae, C. D. A guide to the metabolic pathways and function of metabolites observed in human brain 1H magnetic resonance spectra. *Neurochemical research* **39**, 1-36 (2014).

53 Yang, J. *et al.* Molecular mechanisms underlying human spatial cognitive ability revealed with neurotransmitter and transcriptomic mapping. *Cereb Cortex* **33**, 11320-11328, doi:10.1093/cercor/bhad368 (2023).

54 Ren, J. *et al.* Unraveling neurotransmitter changes in de novo GBA-related and idiopathic Parkinson's disease. *Neurobiol Dis* **185**, 106254, doi:10.1016/j.nbd.2023.106254 (2023).

55 Chen, Z. *et al.* Cortical gradient perturbation in attention deficit hyperactivity disorder correlates with neurotransmitter-, cell type-specific and chromosome- transcriptomic signatures. *Psychiatry Clin Neurosci*, doi:10.1111/pcn.13649 (2024).

56 Premi, E. *et al.* Unravelling neurotransmitters impairment in primary progressive aphasias. *Hum Brain Mapp* **44**, 2245-2253, doi:10.1002/hbm.26206 (2023).

57 Hansen, J. Y. *et al.* Local molecular and global connectomic contributions to cross-disorder cortical abnormalities. *Nat Commun* **13**, 4682, doi:10.1038/s41467-022-32420-y (2022).

58 Stagg, C. J. Magnetic Resonance Spectroscopy as a tool to study the role of GABA in motor-cortical plasticity. *Neuroimage* **86**, 19-27, doi:10.1016/j.neuroimage.2013.01.009 (2014).

59 Hansen, J. Y. *et al.* Mapping neurotransmitter systems to the structural and functional organization of the human neocortex. *Nat Neurosci* **25**, 1569-1581, doi:10.1038/s41593-022-01186-3 (2022).

60 Khan, A. F. *et al.* Patient-specific models link neurotransmitter receptor mechanisms with motor and visuospatial axes of Parkinson's disease. *Nat Commun* **14**, 6009, doi:10.1038/s41467-023-41677-w (2023).

61 Alves, P. N., Forkel, S. J., Corbetta, M. & Thiebaut de Schotten, M. The subcortical and neurochemical organization of the ventral and dorsal attention networks. *Commun Biol* **5**, 1343, doi:10.1038/s42003-022-04281-0 (2022).

62 Sala, A. *et al.* Brain connectomics: time for a molecular imaging perspective? *Trends Cogn Sci* **27**, 353-366, doi:10.1016/j.tics.2022.11.015 (2023).

63 Alexander, L. M. *et al.* An open resource for transdiagnostic research in pediatric mental health and learning disorders. *Scientific data* **4**, 1-26 (2017).

64 Hensch, T. K. Critical period plasticity in local cortical circuits. *Nat Rev Neurosci* **6**, 877-888 (2005).

65 Daucourt, M. C., Erbeli, F., Little, C. W., Haughbrook, R. & Hart, S. A. A meta-analytical review of the genetic and environmental correlations between reading and attention-deficit/hyperactivity disorder symptoms and reading and math. *Scientific Studies of Reading* **24**, 23-56 (2020).

66 Joyner, R. E. & Wagner, R. K. Co-occurrence of reading disabilities and math disabilities: A meta-analysis. *Scientific Studies of Reading* **24**, 14-22 (2020).

67 Beyer, M. *et al.* Structural gray matter features and behavioral preliterate skills predict future literacy - A machine learning approach. *Front Neurosci* **16**, 920150, doi:10.3389/fnins.2022.920150 (2022).

68 Evans, T. M. *et al.* Brain Structural Integrity and Intrinsic Functional Connectivity Forecast 6 Year Longitudinal Growth in Children's Numerical Abilities. *J Neurosci* **35**, 11743-11750, doi:10.1523/JNEUROSCI.0216-15.2015 (2015).

69 Frye, R. E. *et al.* Surface area accounts for the relation of gray matter volume to reading-related skills and history of dyslexia. *Cereb Cortex* **20**, 2625-2635, doi:10.1093/cercor/bhq010 (2010).

70 Li, Y., Hu, Y., Wang, Y., Weng, J. & Chen, F. Individual structural differences in left inferior parietal area are associated with schoolchildrens' arithmetic scores. *Front Hum Neurosci* **7**, 844, doi:10.3389/fnhum.2013.00844 (2013).

71 Linkersdorfer, J., Lonnemann, J., Lindberg, S., Hasselhorn, M. & Fiebach, C. J. Grey matter alterations co-localize with functional abnormalities in developmental dyslexia: an ALE meta-analysis. *PLoS One* **7**, e43122, doi:10.1371/journal.pone.0043122 (2012).

72 Lubin, A. *et al.* Numerical Transcoding Proficiency in 10-Year-Old Schoolchildren is Associated with Gray Matter Inter-Individual Differences: A Voxel-Based Morphometry Study. *Front Psychol* **4**, 197, doi:10.3389/fpsyg.2013.00197 (2013).

73 McCaskey, U., von Aster, M., O'Gorman, R. & Kucian, K. Persistent Differences in Brain Structure in Developmental Dyscalculia: A Longitudinal Morphometry Study. *Front Hum Neurosci* **14**, 272, doi:10.3389/fnhum.2020.00272 (2020).

74 Price, G. R., Wilkey, E. D., Yeo, D. J. & Cutting, L. E. The relation between 1st grade grey matter volume and 2nd grade math competence. *Neuroimage* **124**, 232-237, doi:10.1016/j.neuroimage.2015.08.046 (2016).

75 Skeide, M. A. *et al.* NRSN1 associated grey matter volume of the visual word form area reveals dyslexia before school. *Brain* **139**, 2792-2803, doi:10.1093/brain/aww153 (2016).

76 Starke, M. *et al.* Brain structure, number magnitude processing, and math proficiency in 6- to 7-year-old children born prematurely: a voxel-based morphometry study. *Neuroreport* **24**, 419-424, doi:10.1097/WNR.0b013e32836140ed (2013).

77 Suarez-Pellicioni, M., Soylu, F. & Booth, J. R. Gray matter volume in left intraparietal sulcus predicts longitudinal gains in subtraction skill in elementary school. *Neuroimage* **235**, 118021, doi:10.1016/j.neuroimage.2021.118021 (2021).

78 Torre, G. A. & Eden, G. F. Relationships between gray matter volume and reading ability in typically developing children, adolescents, and young adults. *Dev Cogn Neurosci* **36**, 100636, doi:10.1016/j.dcn.2019.100636 (2019).

79 Viesel-Nordmeyer, N. & Prado, J. Arithmetic skills are associated with left fronto-temporal gray matter volume in 536 children and adolescents. *NPJ Sci Learn* **8**, 56, doi:10.1038/s41539-023-00201-x (2023).

80 Xie, Y. *et al.* Long-term abacus training gains in children are predicted by medial temporal lobe anatomy and circuitry. *Dev Sci*, e13489, doi:10.1111/desc.13489 (2024).

81 Langensee, L., Spotorno, N. & Mårtensson, J. Beyond the language network: Associations between reading, receptive vocabulary, and grey matter volume in 10-year-olds. *Neuropsychologia* **191**, 108719 (2023).

82 Jolles, D. *et al.* Parietal hyper-connectivity, aberrant brain organization, and circuit-based biomarkers in children with mathematical disabilities. *Dev Sci* **19**, 613-631, doi:10.1111/desc.12399 (2016).

83 Li, F. & Tsien, J. Z. Memory and the NMDA Receptors. *New England Journal of Medicine* **361**, 302-303, doi:10.1056/NEJMcibr0902052 (2009).

84 Dupuis, J. P., Nicole, O. & Groc, L. NMDA receptor functions in health and disease: Old actor, new dimensions. *Neuron* **111**, 2312-2328 (2023).

85 Isaacs, E. B., Edmonds, C. J., Lucas, A. & Gadian, D. G. Calculation difficulties in children of very low birthweight: A neural correlate. *Brain* **124**, 1701–1707 (2001).

86 Liu, J. *et al.* Neuroanatomical, transcriptomic, and molecular correlates of math ability and their prognostic value for predicting learning outcomes. *Science Advances* **10**, eadk7220, doi:10.1126/sciadv.adk7220 (2024).

87 Rotzer, S. *et al.* Optimized voxel-based morphometry in children with developmental dyscalculia. *Neuroimage* **39**, 417-422, doi:10.1016/j.neuroimage.2007.08.045 (2008).

88 Rykhlevskaia, E., Uddin, L. Q., Kondos, L. & Menon, V. Neuroanatomical correlates of developmental dyscalculia: combined evidence from morphometry and tractography. *Front Hum Neurosci* **3**, 51, doi:10.3389/neuro.09.051.2009 (2009).

89 González-Burgos, G. *et al.* Distinct properties of layer 3 pyramidal neurons from prefrontal and parietal areas of the monkey neocortex. *Journal of Neuroscience* **39**, 7277-7290 (2019).

90 Perdue, M. V., Mednick, J., Pugh, K. R. & Landi, N. Gray Matter Structure Is Associated with Reading Skill in Typically Developing Young Readers. *Cereb Cortex* **30**, 5449-5459, doi:10.1093/cercor/bhaa126 (2020).

91 Lee, M. M. & Stoodley, C. J. Neural bases of reading fluency: A systematic review and meta-analysis. *Neuropsychologia* **202**, 108947, doi:10.1016/j.neuropsychologia.2024.108947 (2024).

92 Dehaene, S., Cohen, L., Morais, J. & Kolinsky, R. Illiterate to literate: behavioural and cerebral changes induced by reading acquisition. *Nat Rev Neurosci* **16**, 234-244, doi:10.1038/nrn3924 (2015).

93 Chen, L. *et al.* The visual word form area (VWFA) is part of both language and attention circuitry. *Nature communications* **10**, 5601 (2019).

94 Wandell, B. A. & Yeatman, J. D. Biological development of reading circuits. *Current Opinion in Neurobiology* **23**, 261-268 (2013).

95 Del Tufo, S. N. *et al.* Neurochemistry Predicts Convergence of Written and Spoken Language: A Proton Magnetic Resonance Spectroscopy Study of Cross-Modal Language Integration. *Front Psychol* **9**, 1507, doi:10.3389/fpsyg.2018.01507 (2018).

96 Fagerberg, L. *et al.* Analysis of the human tissue-specific expression by genome-wide integration of transcriptomics and antibody-based proteomics. *Mol Cell Proteomics* **13**, 397-406, doi:10.1074/mcp.M113.035600 (2014).

97 Sun, J., Liu, Y., Baudry, M. & Bi, X. SK2 channel regulation of neuronal excitability, synaptic transmission, and brain rhythmic activity in health and diseases. *Biochim Biophys Acta Mol Cell Res* **1867**, 118834, doi:10.1016/j.bbamcr.2020.118834 (2020).

98 de Kovel, C. G. F. *et al.* Neurodevelopmental Disorders Caused by De Novo Variants in KCNB1 Genotypes and Phenotypes. *JAMA Neurol* **74**, 1228-1236, doi:10.1001/jamaneurol.2017.1714 (2017).

99 Lee, J. J. *et al.* Gene discovery and polygenic prediction from a genome-wide association study of educational attainment in 1.1 million individuals. *Nat Genet* **50**, 1112-1121, doi:10.1038/s41588-018-0147-3 (2018).

100 Debanne, D., Inglebert, Y. & Russier, M. Plasticity of intrinsic neuronal excitability. *Curr Opin Neurobiol* **54**, 73-82, doi:10.1016/j.conb.2018.09.001 (2019).

101 Nanou, E. & Catterall, W. A. Calcium Channels, Synaptic Plasticity, and Neuropsychiatric Disease. *Neuron* **98**, 466-481, doi:10.1016/j.neuron.2018.03.017 (2018).

102 Ngo-Anh, T. J. *et al.* SK channels and NMDA receptors form a Ca2+-mediated feedback loop in dendritic spines. *Nat Neurosci* **8**, 642-649, doi:10.1038/nn1449 (2005).

103 Mochel, F. *et al.* Variants in the SK2 channel gene (KCNN2) lead to dominant neurodevelopmental movement disorders. *Brain* **143**, 3564-3573, doi:10.1093/brain/awaa346 (2020).

104 Volk, L., Chiu, S. L., Sharma, K. & Huganir, R. L. Glutamate synapses in human cognitive disorders. *Annu Rev Neurosci* **38**, 127-149, doi:10.1146/annurev-neuro-071714-033821 (2015).

105 Wang, R. & Reddy, P. H. Role of Glutamate and NMDA Receptors in Alzheimer's Disease. *J Alzheimers Dis* **57**, 1041-1048, doi:10.3233/JAD-160763 (2017).

106 Abreu, A. P. & Kaiser, U. B. Pubertal development and regulation. *Lancet Diabetes Endocrinol* **4**, 254-264, doi:10.1016/S2213-8587(15)00418-0 (2016).

107 Blackmon, K. *et al.* Phonetically irregular word pronunciation and cortical thickness in the adult brain. *Neuroimage* **51**, 1453-1458, doi:10.1016/j.neuroimage.2010.03.028 (2010).

108 Herlenius, E. & Lagercrantz, H. Development of neurotransmitter systems during critical periods. *Exp Neurol* **190 Suppl 1**, S8-21, doi:10.1016/j.expneurol.2004.03.027 (2004).

109 Pisters, M. (HOGREFE VERLAG MERKELSTRASSE 3, GOTTINGEN, GERMANY, 2022).

110 Wechsler, D. Wechsler Individual Achievement Test–Third Edition (WIAT-III). *Pearson* (2009).

111 Tustison, N. J. *et al.* Large-scale evaluation of ANTs and FreeSurfer cortical thickness measurements. *Neuroimage* **99**, 166-179 (2014).

112 Wechsler, D. Wechsler Abbreviated Intelligence Scale. . *The Psychological Corp* (1999).

113 Wechsler, D. The Wechsler Individual Achievement Test Second Edition (WIAT-II). *The Psychological Corp* (2001).

114 Klein, A. *et al.* Mindboggling morphometry of human brains. *PLoS computational biology* **13**, e1005350 (2017).

115 Fan, L. *et al.* The Human Brainnetome Atlas: A New Brain Atlas Based on Connectional Architecture. *Cereb Cortex* **26**, 3508-3526, doi:10.1093/cercor/bhw157 (2016).

116 Ly, A., Etz, A., Marsman, M. & Wagenmakers, E. J. Replication Bayes factors from evidence updating. *Behav Res Methods* **51**, 2498-2508, doi:10.3758/s13428-018-1092-x (2019).

117 Shirer, W. R., Ryali, S., Rykhlevskaia, E., Menon, V. & Greicius, M. D. Decoding subject-driven cognitive states with whole-brain connectivity patterns. *Cereb Cortex* **22**, 158-165, doi:10.1093/cercor/bhr099 (2012).

118 Vos de Wael, R. *et al.* BrainSpace: a toolbox for the analysis of macroscale gradients in neuroimaging and connectomics datasets. *Communications biology* **3**, 103 (2020).

119 Zhang, Y., Chang, H., El-Said, D. & Menon, V. Glutamatergic signaling underlies brain structural organization for mathematical and reading abilities in children. *Zenodo*, doi:10.5281/zenodo.20574388 (2026).

Funding

This research was supported by National Institutes of Health grants HD094623, HD059205, MH084164, and MH121069 (VM) and the Stanford Maternal & Child Health Research Institute Postdoctoral Support Award (HC).

Author contributions

Conceptualization: YZ, VM; Methodology: YZ, VM; Formal analysis: YZ, DE; Investigation: YZ, HC, VM; Data curation: YZ, DE; Visualization: YZ; Supervision: VM; Resources: VM; Funding acquisition: VM; Project administration: VM; Writing – original draft: YZ, HC, VM; Writing – review & editing: YZ, HC, DE, VM.

Competing interests

The authors declare no competing interest.

Table 1. Demographics and neuropsychological assessment scores of the CMI-HBN discovery and Stanford validation cohorts

	CMI-HBN Cohort	Stanford Cohort	Group Difference
Sample Size	760	231	—
Age range (years)	7.0 ~ 14.0	7.1 ~ 13.8	—
Age (mean ± SD; years)	9.7 ± 1.8	9.2 ± 1.6	$t(989) = 3.59$, $p = 3.5e\text{-}4$, Cohen's $d = 0.27$, 95% CI [0.12, 0.42]
Sex (M/F)	485/275	133/98	$\chi^2(1) = 2.94$, $p = 0.09$, Cramer's $V = 0.04$, 95% CI [0.00, 1.00]
WISC/WASI full-scale IQ	104.4 ± 13.4	113.1 ± 13.4	$t(989) = -8.63$, $p = 2.4e\text{-}17$, Cohen's $d = -0.65$, 95% CI [-0.80, -0.50]
WIAT-II/III numerical operations (standardized score)	103.0 ± 16.0	108.1 ± 19.1	$t(989) = -4.00$, $p = 7.0e\text{-}5$, Cohen's $d = -0.30$, 95% CI [-0.45, -0.15]
WIAT-II/III math reasoning/math problem solving (standardized score)	101.5 ± 16.3	111.8 ± 16.5	$t(989) = -8.38$, $p = 1.8e\text{-}16$, Cohen's $d = -0.63$, 95% CI [-0.78, -0.48]
WIAT-II/III word reading (standardized score)	104.4 ± 15.4	109.7 ± 11.4	$t(989) = -4.92$, $p = 1.0e\text{-}6$, Cohen's $d = -0.37$, 95% CI [-0.52, -0.22]
WIAT-II/III reading comprehension (standardized score)	102.0 ± 13.4	108.8 ± 11.1	$t(989) = -7.08$, $p = 2.7e\text{-}12$, Cohen's $d = -0.53$, 95% CI [-0.68, -0.38]

Values are presented as mean ± SD unless otherwise indicated. Group differences were assessed using two-sided independent-samples t tests for continuous variables and two-sided chi-square tests for sex. Abbreviations: WISC, Wechsler Intelligence Scale for Children; WASI, Wechsler Abbreviated Scale of Intelligence; WIAT-II/III, Wechsler Individual Achievement Test, Second/Third Edition; SD, standard deviation; CI: confidence interval.

Figure Legends

Fig. 1. Study overview of neurotransmitter mapping to brain structural organization associated with mathematical and reading abilities in children. We used a two-stage analytical approach in two independent cohorts of children aged 7-14 years: the CMI-HBN discovery cohort (*N*=760) and the Stanford validation cohort (*N*=231). Structural MRI images from both cohorts were processed using Advanced Normalization Tools (ANTs), and regional grey matter volume (GMV) values were extracted using the Brainnetome atlas. GMV values and measures of mathematical and reading abilities were used in subsequent analyses. First, we conducted brain-behavior analyses using canonical correlation analysis (CCA) to identify whole-brain structural phenotypes associated with mathematical and reading abilities in each cohort. This yielded spatial maps of brain regions whose GMV collectively covaried with academic performance. Second, we performed neurotransmitter mapping analyses to test how 19 neurotransmitter receptors and transporters related to the spatial expression of CCA-derived brain structural phenotypes. Linear regression models with spatial autocorrelation-preserving permutation tests were used to identify neurotransmitter systems that mapped most strongly onto brain structural organization associated with each academic domain. Blue schematic elements indicate mathematical measures, and orange schematic elements indicate reading measures. Brain maps schematically illustrate CCA-derived GMV weight maps. ANTs = Advanced Normalization Tools; CCA = canonical correlation analysis; GMV = grey matter volume; MRI = magnetic resonance imaging; numop = numerical operations; mathprob = math problem solving; mathreas = math reasoning; reading comp = reading comprehension.

Fig. 2. Multivariate associations between mathematical ability and grey matter volume replicate across independent cohorts. Canonical correlation analysis (CCA) identified mathematical ability-related modes in both **(a)** the CMI-HBN discovery cohort and **(b)** the Stanford validation cohort. Scatter plots show associations between brain and behavioral canonical variates. Shaded bands indicate 95% confidence intervals around the fitted values from linear regression models. Statistical significance of canonical correlations was assessed using upper-tail permutation tests with 5,000 iterations, with FDR correction applied across canonical modes within each cohort. Pearson's *r* and exact FDR-corrected permutation *p* values are shown in each scatter plot. Color squares along the behavioral axis show correlations between the behavioral canonical variate and the original behavioral measures: age, numerical operations, and math problem solving/reasoning. Brain plots show correlations between regional grey matter volume (GMV) and the brain canonical variate across 218 Brainnetome regions of interest. Warmer colors indicate stronger positive GMV loadings; cooler colors indicate weaker loadings. L = left hemisphere; R= right hemisphere; numop = numerical operations; mathprob = math problem solving; mathreas = math reasoning. Source data are provided as a Source Data file.

Fig. 3. Generalizability of brain-behavior associations across independent cohorts. The Canonical Correlation Analysis (CCA) models derived from the CMI-HBN discovery cohort were applied to the independent Stanford validation cohort to predict associations between brain structure and academic abilities. **(a)** Cross-prediction of the relationship between grey matter volume (GMV) and mathematical ability. **(b)** Cross-prediction of the relationship between GMV and reading ability. Scatter plots show correlations between predicted GMV scores and predicted academic performance scores in the Stanford validation cohort. Points represent individual

participants. Shaded bands indicate 95% confidence intervals around the fitted values from linear regression models. Pearson's *r* and exact permutation *p* values are shown in each panel. Statistical significance of the correlations between predicted GMV scores and predicted academic performance scores was assessed using upper-tail permutation tests with 5,000 iterations. Source data are provided as a Source Data file.

Fig. 4. NMDA receptors consistently map onto brain structural organization associated with mathematical ability across cohorts. Linear regression analyses tested associations between 19 neurotransmitter receptors and transporters and math-related CCA-derived brain structural phenotype in **(a)** the CMI-HBN discovery cohort and **(b)** the Stanford validation cohort. Bar lengths represent adjusted R^2 values from the linear regression models. Statistical significance was assessed using upper-tail spatial autocorrelation-preserving spin tests with 5,000 permutations, and FDR correction was applied across neurotransmitter maps. Reported *p* values are FDR-corrected spin-test *p* values. Dark orange bars indicate strong evidence of association, defined as FDR-corrected spin-test $p < 0.05$ and Bayes factor > 3. Light orange bars indicate moderate evidence, defined as either FDR-corrected spin-test $p < 0.05$ or Bayes factor > 3. Grey bars indicate no evidence by these predefined criteria. NMDA receptors, marked with an asterisked, showed robust associations with math-related brain structural organization across both independent cohorts. BF_{10} denotes the Bayes factor in the discovery cohort; BFr_{10} denotes the replication Bayes factor in the validation cohort. Source data are provided as a Source Data file.

Fig. 5. NMDA receptor density maps onto brain structural organization associated with academic abilities across cohorts. Linear regression analyses showed positive correlations between NMDA receptor density and CCA-derived brain structural phenotypes associated with **(a)** mathematical abilities and **(b)** reading abilities in both the CMI-HBN discovery cohort and the Stanford validation cohort. Scatter plots show robust and consistent associations across Brainnetome regions of interest; each point represents one region. Shaded bands indicate 95% confidence intervals around the fitted values from the linear regression models. Pearson's *r* and adjusted R^2 are shown to summarize the linear association and model fit. Statistical significance was assessed using upper-tail spatial autocorrelation-preserving spin tests with 5,000 permutations, with FDR correction applied across neurotransmitter maps. Reported *p* values are FDR-corrected spin-test *p* values. Source data are provided as a Source Data file.

Fig. 6. Network-level associations between NMDA receptor distribution and academic ability-related brain structural organization. NMDA receptor density showed positive correlations with math-related brain structural organization across multiple functional networks in both cohorts: **(a)** dorsal default mode network, **(b)** anterior salience network, **(c)** posterior salience network, and **(d)** higher-order visual network. For reading-related brain structural organization, NMDA receptor density showed consistent positive correlations in (**e**) the higher-order visual network across both cohorts. Scatter plots show associations across Brainnetome regions of interest within each functional network; each point represents one region. Shaded bands indicate 95% confidence intervals around the fitted values from linear regression models. Statistical significance was assessed using two-sided Pearson correlation tests within each network. In the CMI-HBN discovery cohort, FDR correction was applied across all tested

networks. In the Stanford validation cohort, replication analyses were restricted to networks that were significant in the CMI-HBN cohort, and FDR correction was applied across those tested replication networks. Reported *p* values are FDR-corrected *p* values. dDMN = dorsal default mode network; aSalience = anterior salience network; pSalience = posterior salience network; High Visual = higher-order visual network. Source data are provided as a Source Data file.

Fig. 7. Multivariate associations between reading ability and grey matter volume replicate across independent cohorts. Canonical correlation analysis (CCA) identified reading ability-related modes in both (**a**) the CMI-HBN discovery cohort and (**b**) the Stanford validation cohort. Scatter plots show associations between brain and behavioral canonical variates. Shaded bands indicate 95% confidence interval around the fitted values from linear regression models. Statistical significance of canonical correlations was assessed using upper-tail permutation tests with 5,000 iterations, with FDR correction applied across canonical modes within each cohort. Pearson's *r* and exact FDR-corrected permutation *p* values are shown in each scatter plot. Color squares along the behavioral axis show correlations between the behavioral canonical variate and the original behavioral measures: age, word reading, and reading comprehension. Brain plots show correlations between regional grey matter volume (GMV) and the brain canonical variate across 218 Brainnetome regions of interest. Warmer colors indicate stronger positive GMV loadings; cooler colors indicate weaker loadings. L = left hemisphere; R = right hemisphere; wordread = word reading; readcp = reading comprehension. Source data are provided as a Source Data file.

Fig. 8. NMDA receptors consistently map onto brain structural organization associated with reading ability across cohorts. Linear regression analyses tested associations between 19 neurotransmitter receptors and transporters and reading-related CCA-derived brain structural phenotype in **(a)** the CMI-HBN discovery cohort and **(b)** the Stanford validation cohort. Bar lengths represent adjusted R^2 values from the linear regression models. Statistical significance was assessed using upper-tail spatial autocorrelation-preserving spin tests with 5,000 permutations, and FDR correction was applied across neurotransmitter maps. Reported *p* values are FDR-corrected spin-test *p* values. Dark orange bars indicate strong evidence of association, defined as FDR-corrected spin-test $p < 0.05$ and Bayes factor > 3. Light orange bars indicate moderate evidence, defined as either FDR-corrected spin-test $p < 0.05$ or Bayes factor > 3. Grey bars indicate no evidence by these predefined criteria. NMDA receptors, marked with an asterisked, showed robust associations with reading-related brain structural organization across both independent cohorts. BF_{10} denotes the Bayes factor in the discovery cohort; BFr_{10} denotes the replication Bayes factor in the validation cohort. Source data are provided as a Source Data file.

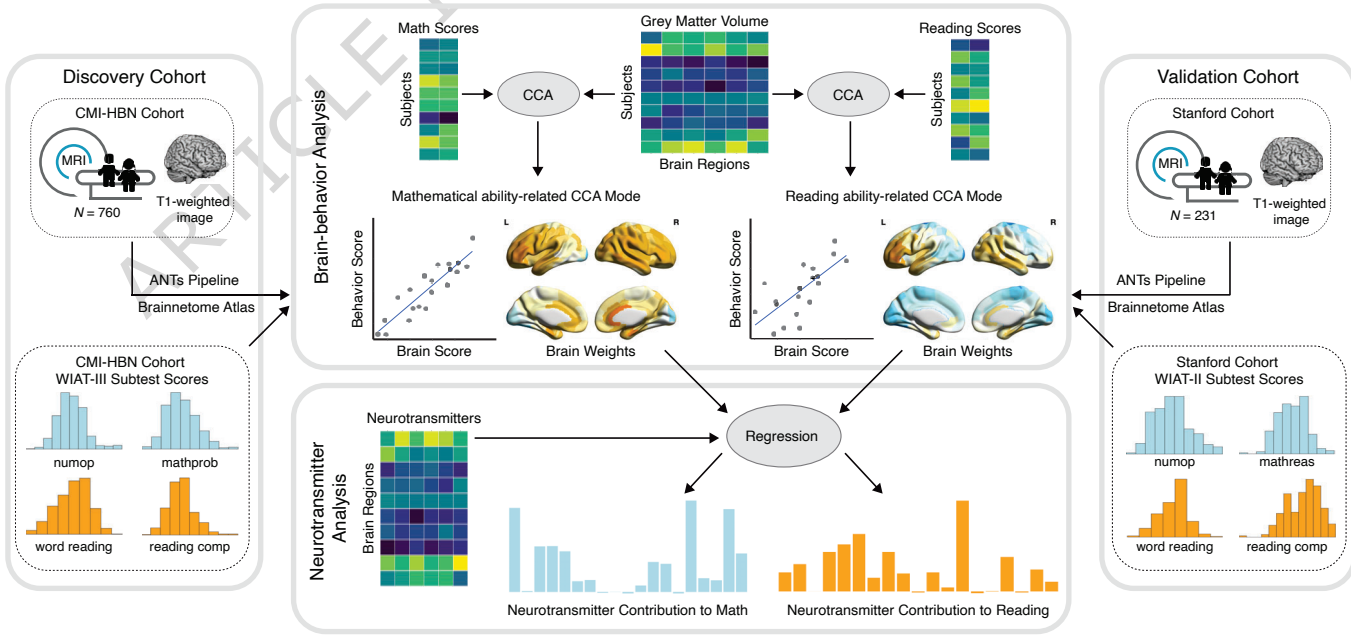

a

Mathematical ability-related CCA mode (CMI-HBN)

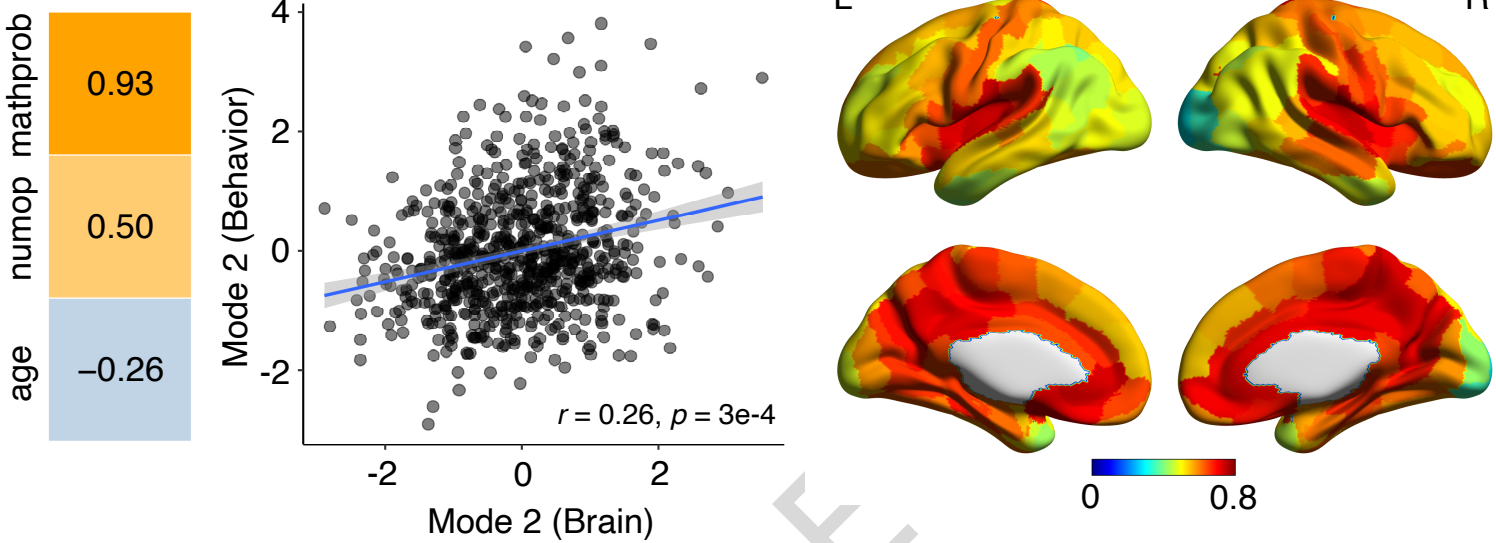

b

Mathematical ability-related CCA mode (Stanford)

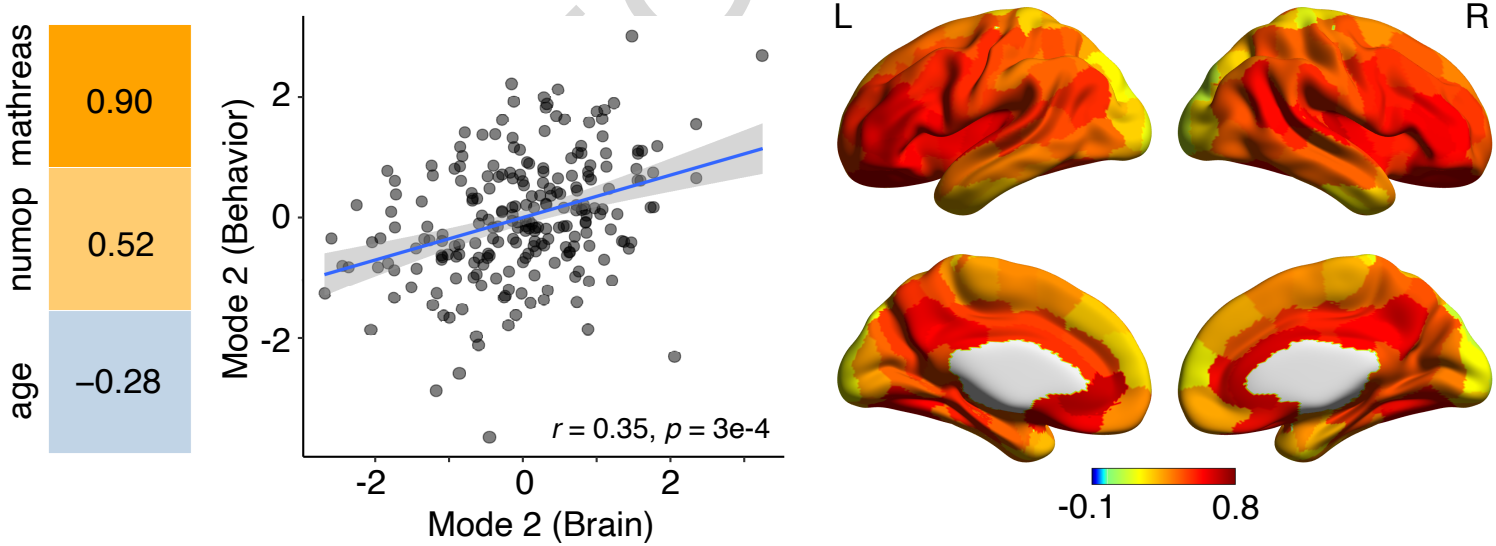

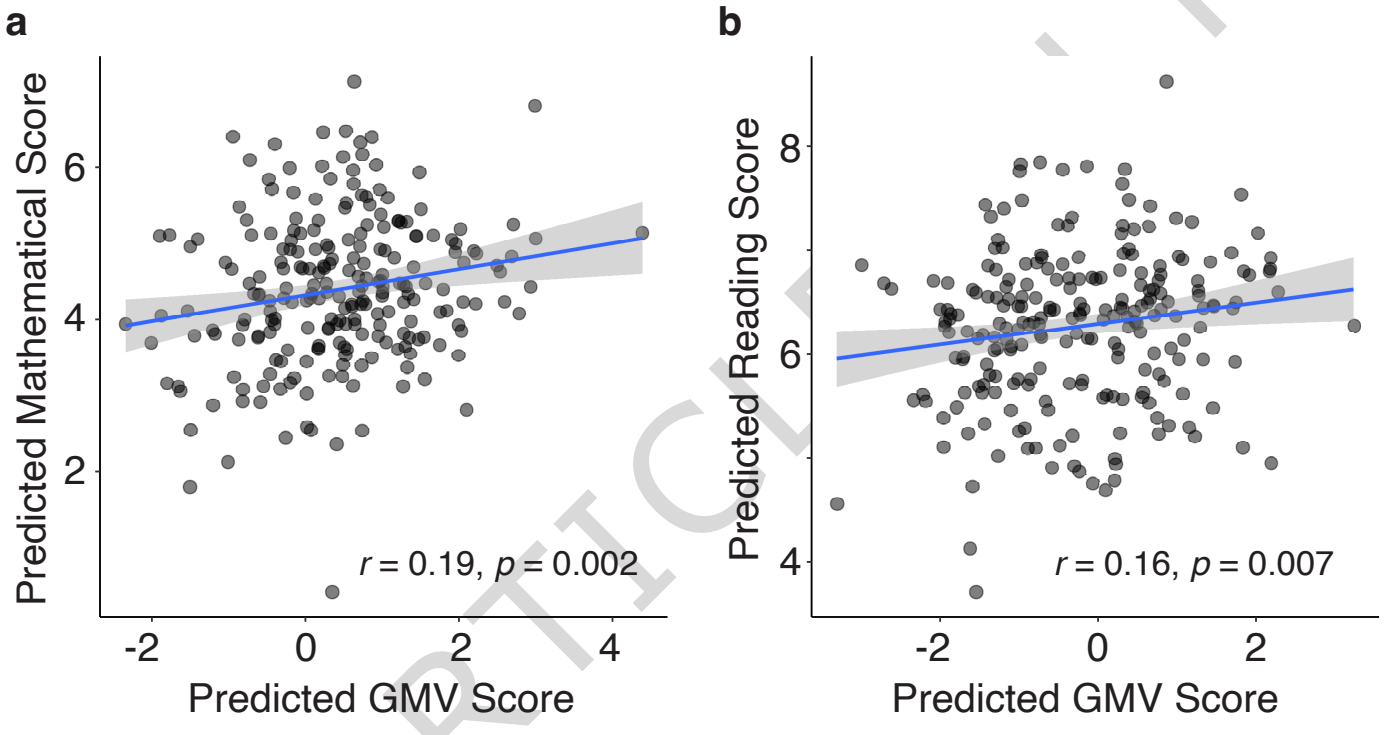

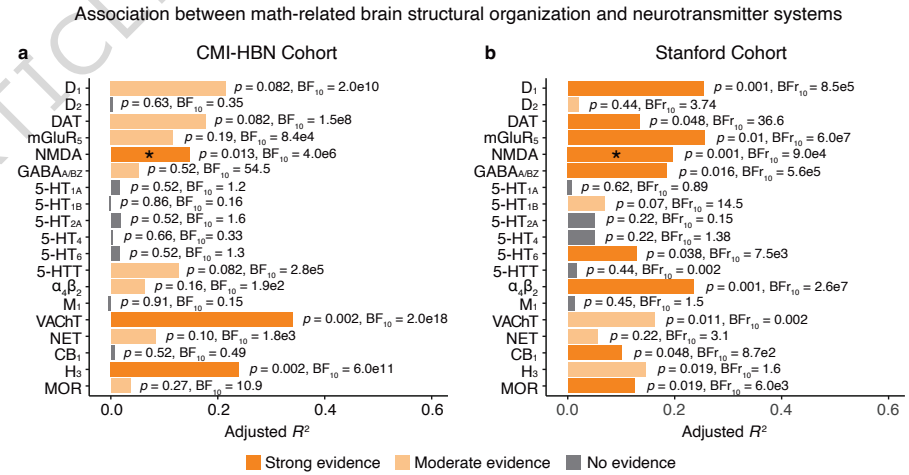

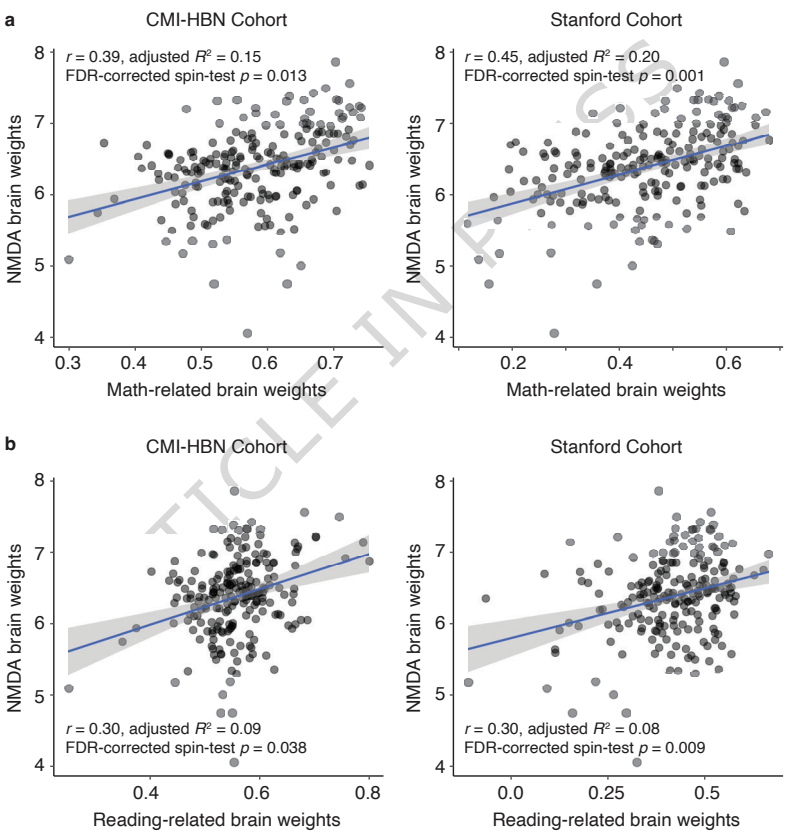

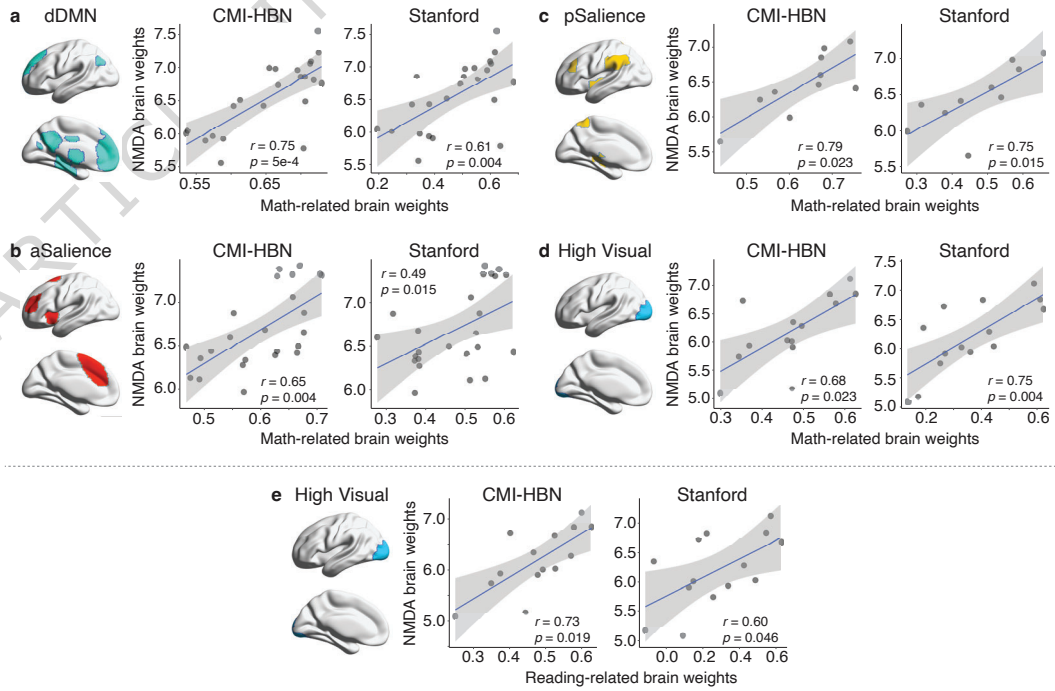

a

Reading ability-related CCA mode (CMI-HBN)

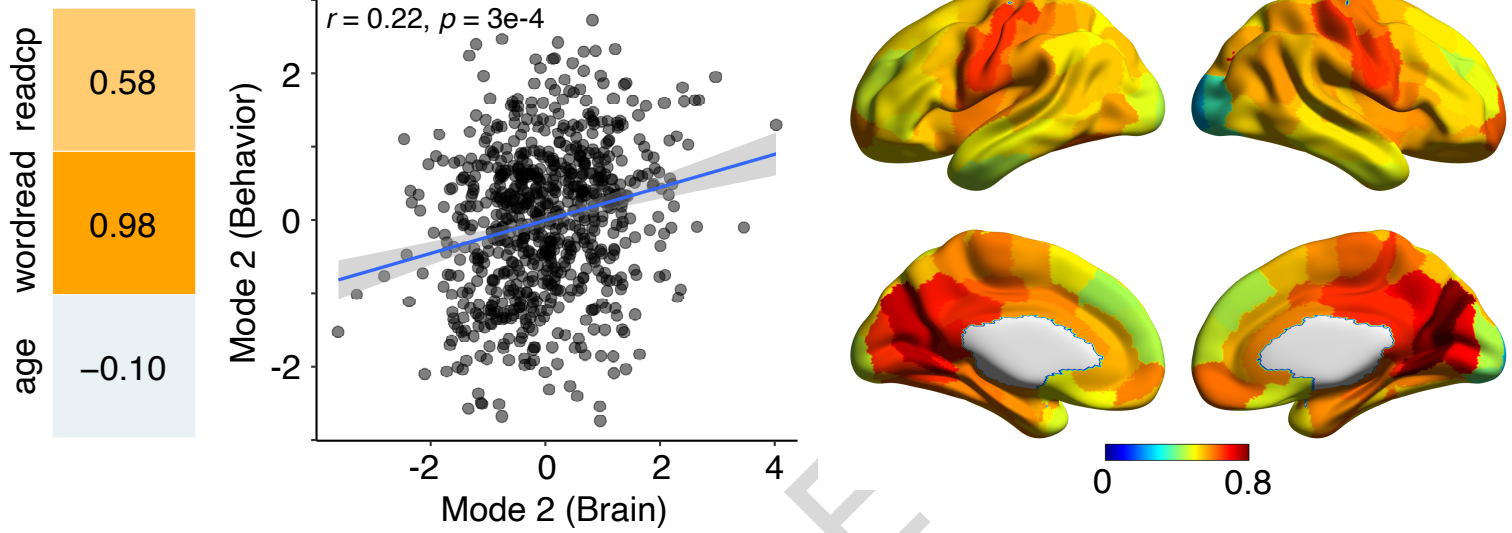

b

Reading ability-related CCA mode (Stanford)